(12) INTERNATIONAL APPLICATION PUBLISHED UNDER THE PATENT COOPERATION TREATY (PCT)

(19) World Intellectual Property Organization
International Bureau

(43) International Publication Date
5 February 2015 (05.02.2015)

WIPO | PCT

(10) International Publication Number
WO 2015/016779 A1

(51) International Patent Classification:
B82Y 30/00 (2011.01) ***C02F 1/44*** (2006.01)
B82B 3/00 (2006.01) ***C01G 21/00*** (2006.01)
B01J 21/06 (2006.01)

(21) International Application Number:
PCT/SG2014/000358

(22) International Filing Date:
29 July 2014 (29.07.2014)

(25) Filing Language: English

(26) Publication Language: English

(30) Priority Data:
61/859,352 29 July 2013 (29.07.2013) US

(71) Applicant: **NATIONAL UNIVERSITY OF SINGAPORE** [SG/SG]; 21 Lower Kent Ridge Road, Singapore 119077 (SG).

(72) Inventors: **LI, Fong Yau Sam**; c/o National University of Singapore, Faculty of Science, Department of Chemistry, 21 Lower Kent Ridge Road, Singapore 119077 (SG). **LIN, Xuanhao**; c/o National University of Singapore, Faculty of Science, Department of Chemistry, 21 Lower Kent Ridge Road, Singapore 119077 (SG).

(74) Agent: **KINNAIRD, James Welsh**; Marks & Clerk Singapore LLP, Tanjong Pagar, P O Box 636, Singapore 910816 (SG).

(81) Designated States *(unless otherwise indicated, for every kind of national protection available)*: AE, AG, AL, AM, AO, AT, AU, AZ, BA, BB, BG, BH, BN, BR, BW, BY, BZ, CA, CH, CL, CN, CO, CR, CU, CZ, DE, DK, DM, DO, DZ, EC, EE, EG, ES, FI, GB, GD, GE, GH, GM, GT, HN, HR, HU, ID, IL, IN, IR, IS, JP, KE, KG, KN, KP, KR, KZ, LA, LC, LK, LR, LS, LT, LU, LY, MA, MD, ME, MG, MK, MN, MW, MX, MY, MZ, NA, NG, NI, NO, NZ, OM, PA, PE, PG, PH, PL, PT, QA, RO, RS, RU, RW, SA, SC, SD, SE, SG, SK, SL, SM, ST, SV, SY, TH, TJ, TM, TN, TR, TT, TZ, UA, UG, US, UZ, VC, VN, ZA, ZM, ZW.

(84) Designated States *(unless otherwise indicated, for every kind of regional protection available)*: ARIPO (BW, GH, GM, KE, LR, LS, MW, MZ, NA, RW, SD, SL, SZ, TZ, UG, ZM, ZW), Eurasian (AM, AZ, BY, KG, KZ, RU, TJ, TM), European (AL, AT, BE, BG, CH, CY, CZ, DE, DK, EE, ES, FI, FR, GB, GR, HR, HU, IE, IS, IT, LT, LU, LV, MC, MK, MT, NL, NO, PL, PT, RO, RS, SE, SI, SK, SM, TR), OAPI (BF, BJ, CF, CG, CI, CM, GA, GN, GQ, GW, KM, ML, MR, NE, SN, TD, TG).

Declarations under Rule 4.17:

— *of inventorship (Rule 4.17(iv))*

Published:

— *with international search report (Art. 21(3))*

(54) Title: TITANIUM DIOXIDE PHOTOCATALYSTS FOR REVERSE OSMOSIS CONCENTRATE RECOVERY

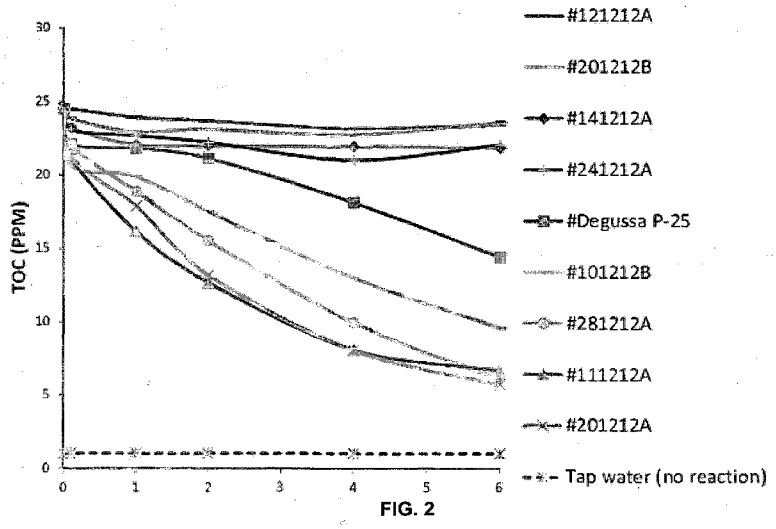


FIG. 2

(57) Abstract: Disclosed herein is a composition comprising: TiO_2 nanocrystals in the form of agglomerates and/or aggregates; and an anionic species associated with the TiO_2 agglomerates/aggregates, wherein the diameter of the TiO_2 agglomerates/aggregates is from 0.02 μm to 5.0 μm; the diameter of the TiO_2 nanocrystals is from 4 to 70 nm; and the BET surface area of the composition is from 6 to 250 g/m^2. There is also disclosed a method for making said compositions and uses thereof.

WO 2015/016779 A1

TITANIUM DIOXIDE PHOTOCATALYSTS FOR REVERSE OSMOSIS CONCENTRATE RECOVERY

Field of Invention

This invention relates to improved TiO_2 compositions for use as photocatalysts in a number of applications, including the purification of wastewater, and methods of making the same.

Background

The listing or discussion of a prior-published document in this specification should not necessarily be taken as an acknowledgement that the document is part of the state of the art or is common general knowledge.

Many cities in the world have wastewater recovery facilities to minimize wastewater discharge and produce clean water for daily usage. Reverse osmosis membrane technology has been widely applied in the wastewater recovery processes, either via conventional process or membrane bioreactor (MBR) process. However, currently only 70-80% of the total volume of the wastewater can be purified and recovered as clean product water using reverse osmosis membrane technology, the remaining 20-30% of the total volume of the wastewater remains as reverse osmosis concentrate, which is a brackish waste that has to be disposed of and, due to its high organic content, it is also harmful to the environment.

Reverse osmosis (RO) concentrate typically contains a few hundred ppm of ionic materials (cations and anions), and 20-30 ppm of organic substances, which make the RO concentrate brownish in colour. Deionization technology is able to remove ions at a relatively high cost (due to the use of a significant amount of electricity to accomplish this task). However, deionization technology is not able to remove the organic materials, some of which may be toxic. Conventional approaches to remove organic substances include activated carbon adsorption and coagulation by aluminum sulfate or ferric chloride. Modern advanced oxidation processes (AOPs) include photocatalysis under UV-visible light or sunlight, ozone oxidation, hydrogen peroxide oxidation, sonolysis (sonication), electrolytic oxidation, and so on. Combined or not combined with other methods, photocatalysis under UV or visible light or sunlight is one of the best ways to remove organic substances from RO concentrate.

Anatase TiO_2 semiconductor has a band gap of more than 3 eV and has been widely used as a catalytic material, for example, as a catalyst or a support material for active metal and metal oxide catalysts. TiO_2 has been successfully applied as a heterogeneous UV-sensitive photocatalyst, which has attracted the attention of people interested in developing new photocatalytic materials at the nano-scale. TiO_2 for water treatment also attracts much research attention due to its low cost, that no additional chemicals are needed, the process is environmental friendly, and the potential ability to conduct the process using direct sunlight. However, currently available photocatalysts, such as the widely referred to Degussa P-25 titanium dioxide, are not entirely satisfactory in the above applications due to low efficiency.

Summary of Invention

This invention discloses highly efficient titanium dioxide TiO_2 photocatalysts able to degrade organic substances in reverse osmosis concentrate (ROC) under UV-visible light or sunlight to improve the ratio of purified water to reverse osmosis membrane product from 70% to greater than or equal to 95%, and at the same time reducing the brackish waste from 30% to less than or equal to 5%.

This invention enables the possibility of producing an additional 200,000 cubic meters (m^3) clean water every day at a minimal cost for a city with a population of 5-million people, having wastewater reclamation facilities ordinarily capable of producing 550,000 cubic meters (m^3) reclaimed water every day, which is 30% of such a city's daily water usage, while also reducing the amount of brackish waste by 200,000 cubic meters (m^3). Since an additional 200,000 cubic meters (m^3) clean water accounts for 11% of such a city's daily water usage, this invention may have significant economic and social advantages for major cities around the world.

In a first aspect of the invention, there is provided a composition comprising TiO_2 nanocrystals in the form of agglomerates and/or aggregates; and an anionic species associated with the TiO_2 agglomerates/aggregates, wherein the diameter of the TiO_2 agglomerates/aggregates is from 0.02 μm to 5.0 μm; the diameter of the TiO_2 nanocrystals is from 4 to 70 nm; and the BET surface area of the composition is from 6 to 250 g/m^2 (e.g. the diameter of the TiO_2 agglomerates/aggregates is from 0.02 μm to 3.0 μm; the diameter of the TiO_2 nanocrystals is from 4 to 70 nm; and the BET surface area of the composition is from 6 to 170 g/m^2).

In embodiments of the invention, the direct band gap of the TiO_2 nanocrystals may be from 3.00 to 3.70 eV (e.g. 3.34 to 3.50 eV) and/or the indirect band gap of the TiO_2 nanocrystals may be from 2.90 to 3.50 eV (3.17 to 3.30 eV). For example, the direct band gap of the TiO_2 nanocrystals may be from 3.35 to 3.45 eV and/or the indirect band gap of the TiO_2 nanocrystals may be from 3.20 to 3.26 eV.

In certain embodiments of the invention, the TiO_2 nanocrystals may be substantially in the anatase form. For example, the TiO_2 nanocrystals may be in the anatase form, though they may contain surface defects and secondary structures.

In yet further embodiments of the invention, the anionic species may be selected from one or more of the group consisting of Cl^-, F^-, Br^-, I^-, PO_4^{3-}, NO_3^-, BO_3^{3-}, SiO_3^{2-} and, more particularly, SO_4^{2-}.

In still further embodiments of the invention, when the anionic species is SO_4^{2-}, Ti may be present in an amount of from 50.9 wt% to 63.9 wt%; and/or O may be present in an amount of from 36.09 wt% to 44.5 wt%; and/or S may be present in an amount of from 0.01 wt% to 4.6 wt% (e.g. Ti may be present in an amount of from 55.9 wt% to 59.49 wt%; and/or O may be present in an amount of from 40.5 wt% to 41.5 wt%; and/or S may be present in an amount of from 0.01 wt% to 2.6 wt%, such as Ti may be present in an amount of from 55.9 wt% to 59.0 wt%; and/or O may be present in an amount of from 40.5 wt% to 41.5 wt%; and/or S may be present in an amount of from 0.5 wt% to 2.6 wt%; or, more particularly, Ti may be present in an amount of from 57.3 wt% to 58.5 wt%; and/or O may be present in an amount of from 40.5 wt% to 40.9 wt%; and/or S may be present in an amount of from 1.0 wt% to 1.8 wt%).

In certain embodiments of the invention, when the anionic species is SO_4^{2-}, the composition may have FTIR peaks at approximately 3620-3850 cm^{-1}, 3159 cm^{-1}, 1400 cm^{-1}, 1215 cm^{-1}, 1148 cm^{-1}, 1051 cm^{-1} and 980 cm^{-1}. Additionally and/or alternatively, the proportion of Ti-OH species compared to $Ti\text{-}OSO_3$ species of the surface of the aggregates/agglomerates, as measured using the Ti $2p_{3/2}$ peaks using X-ray photoelectron spectroscopy, is from 1.5:1 to 2:1; and/or the proportion of Ti-OH species compared to $Ti\text{-}OSO_3$ species of the surface of the aggregates/agglomerates, as measured using the O 1s peaks using X-ray photoelectron spectroscopy, is from 1.5:1 to 2:1; and/or the proportion of Ti-O(O=S=O)O-Ti species compared to Ti-OO(O=S=O) species of the surface of the aggregates/agglomerates, as measured using the S $2p_{3/2}$ peaks using X-ray photoelectron spectroscopy, is from 4:1 to 5:1.

In still further embodiments, the diameter of the agglomerates/aggregates may be from 0.05 μm to 3.0 μm (e.g. from 0.1 μm to 1.0 μm); and/or the diameter of the TiO_2 nanocrystals may be from 5 to 50 nm (e.g. from 5 to 30 nm, such as from 9 to 26 nm or from 5.7 to 6.4 nm).

In yet further embodiments, the BET surface area of the composition may be from 6.0 to 9.0 g/m^2; or the BET surface area of the composition may be from 20.0 to 90.0 g/m^2; or the BET surface area of the composition may be from 115 to 250 g/m^2 (e.g. from 6.5 to 7.0 g/m^2; or the BET surface area of the composition may be from 30.0 to 70.0 g/m^2; or the BET surface area of the composition may be from 145 to 170 g/m^2).

In still further embodiments of the invention, the majority of the anionic species may be associated with the surface of the TiO_2 agglomerates/aggregates. For example, the ratio of the anionic species on the surface of the TiO_2 agglomerates/aggregates compared to the anionic species within the interior volume of the TiO_2 agglomerates/aggregates is from 1.5:1 to 30:1, optionally from 2:1 to 10:1, such as from 3:1 to 8:1 (e.g. from 5:1 to 8:1).

In still further embodiments of the invention, 0.1 wt% of the composition reduces the dissolved organic carbon in 99.9 wt% of reverse osmosis concentrate by from 70% to 80% after 6 hours of photocatalytic reaction.

In a second aspect of the invention, there is provided a method of preparing TiO_2 nanocrystals, the method comprising the steps of:

(a) hydrolysing a titanium source in a water/solvent mixture to form a hydrous TiO_2 material;

(b) filtering the hydrous TiO_2 material and washing the filtered hydrous TiO_2 material with a washing solution;

(c) drying and grinding the filtered and washed hydrous TiO_2 material into a powder;

(d) calcinating the powder to form anhydrous TiO_2 nanocrystals; and

(e) optionally further grinding the anhydrous TiO_2 nanocrystals.

In embodiments of the invention, the titanium source may be one or more of the group selected from titanyl sulfate, $TiCl_3$, $TiCl_4$, oxalotitanic acid, titanium ethoxide, titanium n-propoxide, titanium isopropoxide, and titanium n-butoxide. For example, the titanium source is titanyl sulfate.

In embodiments of the invention, the hydrolysis may be conducted:

a) at from 25 to 190°C, such as from 85 to 95°C, or from 100 to 190°C; and/or

b) using a solvent that is one or more selected from methanol, ethanol, n-propanol, isopropanol, acetone, acetylacetone, methyl ethyl ketone, methyl propyl ketone, methyl isobutyl ketone, methyl pentyl ketone, butyrolactone, methyl formate, ethyl formate, propyl formate, butyl formate, methyl acetate, oxaloacetate, ethyl acetate, propyl acetate, butyl acetate, and dibasic ester (e.g. ethanol); and/or

c) the water/solvent ratio is from 1:10 to 20:1 (e.g. from 2:1 to 4:1), or only water is used.

In still further embodiments of the invention, the washing solution may be selected from one or more of 0.01 to 5 M ammonia (aq), methanol, ethanol, isopropanol, acetone, methyl ethyl ketone, methyl isobutyl ketone, methyl formate, ethyl formate, methyl acetate, and ethyl acetate (e.g. 0.1 M ammonia (aq)).

In yet still further embodiments of the invention, the hydrous TiO_2 material may be dried at a temperature of from 10°C to 100°C for a period of from 0.5 to 24 hours, such as at a temperature of from 40°C to 80°C for a period of from 6 to 12 hours.

In yet further embodiments, the calcination step may be conducted at a temperature of from 100°C to 1000°C using a temperature ramp of from 0.1°C to 100°C per minute for from 0.1 to 48 hours, such as at a temperature of from 250°C to 600°C using a temperature ramp of from 5°C to 15°C per minute (e.g. 10°C per minute) for from 0.5 to 4 hours.

In yet still further embodiments, the weight ratio of the titanium source to the solvent/water in the hydrolysis step may be from 1:1000 to 10:1, such as from 1:100 to 1:10.

In still further embodiments of the invention, the filtering of the hydrolysed material may occur before and/or after the washing step.

In yet still further embodiments of the invention, step (a) may further comprise adding a counterion source to the titanium source and water/solvent mixture, optionally wherein the counterion source contains one or more counterions selected from the group consisting of F^-, Br^-, I^-, PO_4^{3-}, NO_3^-, BO_3^{3-}, and SiO_3^{2-}.

In a third aspect of the invention, there is provided a composition made by the process as described in the aspect and embodiments of the second aspect of the invention.

In a fourth aspect of the invention, there is provided a use of a composition according to the first and third aspects and embodiments of the invention as a photocatalyst. For example, said compositions may be used in the treatment of any one of wastewater, drinking water and ROC; air purification; and surface self-cleaning.

In a fifth aspect of the invention, there is provided a composition comprising:

TiO_2 nanocrystals in the form of agglomerates and/or aggregates; and

an anionic species, wherein the anionic species is SO_4^{2-} and is associated with the TiO_2 agglomerates/aggregates, and wherein:

the composition has FTIR peaks at approximately 3620-3850 cm^{-1}, 3159 cm^{-1}, 1400 cm^{-1}, 1215 cm^{-1}, 1148 cm^{-1}, 1051 cm^{-1} and 980 cm^{-1}; and/or

the content of sulfur in the composition is from 0.01 to 3.0 wt% (e.g. from 0.05 to 2.6 wt%, such as from 0.5 to 1.8 wt%, e.g. from 1.0 to 1.5 wt%); and/or

the proportion of Ti-OH species compared to $Ti\text{-}OSO_3$ species of the surface of the aggregates/agglomerates, as measured using the Ti $2p_{3/2}$ peaks using X-ray photoelectron spectroscopy, is from 1.5:1 to 2:1; and/or

the proportion of Ti-OH species compared to $Ti\text{-}OSO_3$ species of the surface of the aggregates/agglomerates, as measured using the O 1s peaks using X-ray photoelectron spectroscopy, is from 1.5:1 to 2:1; and/or

the proportion of Ti-O(O=S=O)O-Ti species compared to Ti-OO(O=S=O) species of the surface of the aggregates/agglomerates, as measured using the S $2p_{3/2}$ peaks using X-ray photoelectron spectroscopy, is from 4:1 to 5:1.

Embodiments of the fifth aspect of the invention may be the same as those provided in respect of the composition provided in the first aspect of the invention, provided that the embodiment relates to a composition wherein the anionic species is SO_4^{2-}.

The invention may also be described by reference to the following numbered clauses below.

1. A composition comprising:

TiO_2 nanocrystals in the form of agglomerates and/or aggregates; and

an anionic species associated with the TiO_2 agglomerates/aggregates, wherein

the diameter of the TiO_2 agglomerates/aggregates is from 0.02 μm to 5.0 μm (e.g. from 0.02 μm to 3.0 μm);

the diameter of the TiO_2 nanocrystals is from 4 to 70 nm; and

the BET surface area of the composition is from 6 to 250 g/m^2 (e.g. from 6 to 170 g/m^2).

2. The composition according to Clause 1, wherein the direct band gap of the TiO_2 nanocrystals is from 3.00 to 3.70 eV and/or the indirect band gap of the TiO_2 nanocrystals may be from 2.90 to 3.50 eV (e.g. 3.34 to 3.50 eV and/or the indirect band gap of the TiO_2 nanocrystals is from 3.17 to 3.30 eV, such as the direct band gap of the TiO_2 nanocrystals is from 3.35 to 3.45 eV and/or the indirect band gap of the TiO_2 nanocrystals is from 3.20 to 3.26 eV).

3. The composition according to Clause 1 or Clause 2, wherein the TiO_2 nanocrystals are substantially in the anatase form (e.g. the TiO_2 nanocrystals may be in the anatase form, though they may contain surface defects and secondary structures).

4. The composition according to any one of the preceding clauses, wherein the anionic species is selected from one or more of the group consisting of SO_4^{2-}, Cl^-, F^-, Br^-, I^-, PO_4^{3-}, NO_3^-, BO_3^{3-}, and SiO_3^{2-} (e.g. SO_4^{2-}).

5. The composition of Clause 4, wherein:

Ti is present in an amount of from 50.9 wt% to 63.9 wt% (e.g. Ti is present in an amount of from 55.9 wt% to 59.49 wt%); and/or

O is present in an amount of from 36.09 wt% to 44.5 wt% (e.g. O is present in an amount of from 40.5 wt% to 41.5 wt%); and/or

S is present in an amount of from 0.01 wt% to 4.6 wt% (e.g. S is present in an amount of from 0.01 wt% to 2.6 wt%).

6. The composition of Clause 5, wherein:

Ti is present in an amount of from 55.9 wt% to 59.0 wt%; and/or

O is present in an amount of from 40.5 wt% to 41.5 wt%; and/or

S is present in an amount of from 0.5 wt% to 2.6 wt%.

7. The composition of Clause 6, wherein:

Ti is present in an amount of from 57.3 wt% to 58.5 wt%; and/or

O is present in an amount of from 40.5 wt% to 40.9 wt%; and/or

S is present in an amount of from 1.0 wt% to 1.8 wt%.

8. The composition of any one of Clauses 4 to 7, wherein the composition has FTIR peaks at approximately 3620-3850 cm^{-1}, 3159 cm^{-1}, 1400 cm^{-1}, 1215 cm^{-1}, 1148 cm^{-1}, 1051 cm^{-1} and 980 cm^{-1}.

9. The composition of any one of Clauses 4 to 9, wherein:

the proportion of Ti-OH species compared to Ti-OSO_3 species of the surface of the aggregates/agglomerates, as measured using the Ti $2p_{3/2}$ peaks using X-ray photoelectron spectroscopy, is from 1.5:1 to 2:1; and/or

the proportion of Ti-OH species compared to Ti-OSO_3 species of the surface of the aggregates/agglomerates, as measured using the O 1s peaks using X-ray photoelectron spectroscopy, is from 1.5:1 to 2:1; and/or

the proportion of Ti-O(O=S=O)O-Ti species compared to Ti-OO(O=S=O) species of the surface of the aggregates/agglomerates, as measured using the S $2p_{3/2}$ peaks using X-ray photoelectron spectroscopy, is from 4:1 to 5:1.

10. The composition according to any one of the preceding clauses, wherein:

the diameter of the agglomerates/aggregates is from 0.05 µm to 3.0 µm (e.g. from 0.1 µm to 1.0 µm); and/or

the diameter of the TiO_2 nanocrystals is from 5 to 50 nm (e.g. from 5 to 30 nm, such as from 9 to 26 nm or 5.7 to 6.4 nm).

11. The composition according to any one of the preceding clauses, wherein the BET surface area of the composition is from 6.0 to 9.0 g/m^2; or the BET surface area of the composition is from 20.0 to 90.0 g/m^2; or the BET surface area of the composition is from 115 to 250 g/m^2 (e.g. from 6.5 to 7.0 g/m^2; or the BET surface area of the composition may be from 30.0 to 70.0 g/m^2; or the BET surface area of the composition may be from 145 to 170 g/m^2).

12. The composition according to any one of the preceding clauses, wherein the majority of the anionic species is associated with the surface of the TiO_2 agglomerates/aggregates.

13. The composition according to Clause 12, wherein the ratio of the anionic species on the surface of the TiO_2 agglomerates/aggregates compared to the anionic species within the

interior volume of the TiO_2 agglomerates/aggregates is from 1.5:1 to 30:1, optionally from 2:1 to 10:1, such as from 3:1 to 8:1 (e.g. from 5:1 to 8:1).

14. The composition according to any one of the preceding clauses, wherein 0.1 wt% of the composition reduces the dissolved organic carbon in 99.9 wt% of reverse osmosis concentrate by from 70% to 80% after 6 hours of photocatalytic reaction.

15. A method of preparing TiO_2 nanocrystals, the method comprising the steps of:

(a) hydrolysing a titanium source in a water/solvent mixture to form a hydrous TiO_2 material;

(b) filtering the hydrous TiO_2 material and washing the filtered hydrous TiO_2 material with a washing solution;

(b) drying and grinding the filtered and washed hydrous TiO_2 material into a powder;

(c) calcinating the powder to form anhydrous TiO_2 nanocrystals; and

(d) optionally further grinding the anhydrous TiO_2 nanocrystals.

16. The method of Clause 15, wherein the titanium source is one or more of the group selected from titanyl sulfate, $TiCl_3$, $TiCl_4$, oxalotitanic acid, titanium ethoxide, titanium n-propoxide, titanium isopropoxide, and titanium n-butoxide (e.g. titanyl sulfate).

17. The method of Clause 15 or Clause 16, wherein:

a) the hydrolysis is conducted at from 25 to 190°C, such as from 85 to 95°C or from 100 to 190°C; and/or

b) the solvent used in the hydrolysis reaction is one or more selected from methanol, ethanol, n-propanol, isopropanol, acetone, acetylacetone, methyl ethyl ketone, methyl propyl ketone, methyl isobutyl ketone, methyl pentyl ketone, butyrolactone, methyl formate, ethyl formate, propyl formate, butyl formate, methyl acetate, oxaloacetate, ethyl acetate, propyl acetate, butyl acetate, and dibasic ester (e.g. ethanol); and/or

c) the water/solvent ratio is from 1:10 to 20:1 (e.g. from 2:1 to 4:1), or only water is used; and/or

d) the washing solution is selected from one or more of 0.01 to 5 M ammonia (aq), methanol, ethanol, isopropanol, acetone, methyl ethyl ketone, methyl isobutyl ketone, methyl formate, ethyl formate, methyl acetate, and ethyl acetate (e.g. 0.1 M ammonia (aq));

e) the hydrous TiO_2 material is dried at a temperature of from 10°C to 100°C for a period of from 0.5 to 24 hours, such as at a temperature of from 40°C to 80°C for a period of from 6 to 12 hours; and/or

f) the calcination step is conducted at a temperature of from 100°C to 1000°C using a temperature ramp of from 0.1°C to 100°C per minute for from 0.1 to 48 hours, such as at a temperature of from 250°C to 600°C using a temperature ramp of from 5°C to 15°C per minute (e.g. 10°C per minute) for from 0.5 to 4 hours; and/or

g) the weight ratio of the titanium source to the solvent/water in the hydrolysis step is from 1:1000 to 10:1, such as from 1:100 to 1:10; and/or

h) the filtering of the hydrolysed material occurs before and/or after the washing step.

18. The method of any one of Clauses 15 to 17, wherein step (a) further comprises adding a counterion source to the titanium source and water/solvent mixture, optionally wherein the counterion source contains one or more counterions selected from the group consisting of F^-, Br^-, I^-, PO_4^{3-}, NO_3^-, BO_3^{3-}, and SiO_3^{2-}.

19. A composition made by the process of any one of Clauses 15 to 18.

20. Use of the composition of any one of Clauses 1-14 and 19 as a photocatalyst (e.g. wherein the composition is used in the treatment of any one of wastewater, drinking water and ROC; and/or air purification; and/or surface self-cleaning).

The invention may be further described in respect of the aspects and embodiments of the invention in the following lettered clauses.

A. A composition comprising:

TiO_2 nanocrystals in the form of agglomerates and/or aggregates; and

an anionic species, wherein:

the anionic species is associated with the TiO_2 agglomerates/aggregates; and

the majority of the anionic species is associated with the surface of the TiO_2 agglomerates/aggregates.

B. The composition of Clause A, wherein the anionic species is selected from one or more of the group consisting of SO_4^{2-}, Cl^-, F^-, Br^-, I^-, PO_4^{3-}, NO_3^-, BO_3^{3-}, and SiO_3^{2-} (e.g. SO_4^{2-}).

C. The composition of any one of the preceding clauses, wherein:

(a) the amount of the anionic species on the surface of the TiO_2 agglomerates/aggregates compared to the anionic species within the interior volume of the TiO_2 agglomerates/aggregates is from 1.5:1 to 30:1, optionally from 2:1 to 10:1, such as from 3:1 to 8:1; and/or

(b) the diameter of the agglomerates/aggregates is from 0.02 μm to 5.0 μm (e.g. 0.02 μm (or 0.05 μm) to 3.0 μm, such as from 0.1 μm to 1.0 μm); and/or

(c) the diameter of the TiO_2 nanocrystals is from 5 to 50 nm (e.g. from 5 to 30 nm, such as from 9 to 26 nm); and/or

(d) the BET surface area of the composition is from 6 to 250 g/m^2 (e.g. from 6.0 to 9.0 g/m^2; or from 20.0 to 90.0 g/m^2; or from 115 to 250 g/m^2 (such as from 6.5 to 7.0 g/m^2; or from 30.0 to 70.0 g/m^2; or from 145 to 170 g/m^2); and/or

(e) the direct band gap of the TiO_2 nanocrystals is from 3.00 to 3.70 eV (e.g. 3.34 to 3.50 eV) and/or the indirect band gap of the TiO_2 nanocrystals may be from 2.90 to 3.50 eV (3.17 to 3.30 eV), optionally wherein the direct band gap of the TiO_2 nanocrystals is from 3.35 to 3.45 eV and the indirect band gap of the TiO_2 nanocrystals is from 3.20 to 3.26 eV; and/or

(f) the TiO_2 nanocrystals are substantially in the anatase form.

Description of Figures

The invention will now be described in further detail below, with the aid of the following figures.

Fig. 1: Photocatalytic reaction set-up for the treatment of reverse osmosis concentrate (ROC).

Fig. 2: Total Organic Concentration (TOC) in ROC following reaction with various photocatalysts for 6 hours.

Fig. 3: TOC in ROC following reaction with E20W80 for 24 hours.

Fig. 4: (a) DOC conversion (C/C_0) of ROC after 6 hours photocatalytic reaction over Degussa P25 pure TiO_2 and SO_4^{2-}/TiO_2 catalyst prepared from different

ethanol/water ratio. Ethanol/water ratio during preparation for E0W100, E20W80, E33W67, E50W50, E67W33, E80W20 and E100W0 are 0/100, 20/80, 33/67, 50/50, 67/33, 80/20 and100/0, respectively. E0W100, E20W80 and E33W67 showed best activity. b) Photoreaction kinetic plot, $\ln(C/C_0)$ versus ROC reaction time t over catalyst E33W67, first order for humic substances. C_0, C – humic substancesfluorescence integration before and after photoreaction. (c) Normalised UV-Vis absorbance at 254 nm after ROC 6 hours photocatalytic reaction over different catalysts; (d) Normalised UV-vis absorbance at 455 nm after ROC 6 hrs' photocatalytic reaction over different catalysts. A455 < 0.1 is colourless to naked eyes.

Fig. 5: Powder X-ray diffraction patterns of SO_4^{2-}/TiO_2 photocatalysts E0W100, E20W80, E33W67, E50W50, E67W33, E80W20, E100W0 and Degussa P25 TiO_2.

Fig. 6: Energy dispersive spectra (EDS) of SO_4^{2-}/TiO_2 photocatalysts (a) E20W80 and (b) E80W20.

Fig. 7: FT-IR spectra of SO_4^{2-}/TiO_2 photocatalysts E20W80, E33W67, E50W50, E67W33, E80W20 and Degussa P25 TiO_2.

Fig. 8: X-ray photoelectron spectra (XPS) of SO_4^{2-}/TiO_2 photocatalysts E33W67 and E80W20; (a) full scan, (b) C 1s (c) Ti 2p, (d) structure depicting various types of Ti (e) O 1s, (e) structure depicting various types of O, (g) S 2p, (h) structure depicting various types of S.

Fig. 9: (a) SEM image of E20W80 SO_4^{2-}/TiO_2 photocatalyst; (b) SEM image of E67W33 SO_4^{2-}/TiO_2 photocatalyst; (c) TEM image of E20W80 SO_4^{2-}/TiO_2 photocatalyst; (d) HRTEM image of E20W80 SO_4^{2-}/TiO_2 photocatalyst; (e) Selected area electron diffraction (SAED) of E20W80 SO_4^{2-}/TiO_2 photocatalyst.

Fig. 10: Depicts the direct and indirect band gaps for E20W80 following calcination for 1 hour and 4 hours at 400°C.

Fig. 11: (a) UV-Vis diffuse reflectance spectra (DRS); (b) Tauc plot for direct band gap; (c) Tauc plot for indirect band gap of SO_4^{2-}/TiO_2 photocatalysts E0W100, E20W80, E33W67, E50W50, E67W33, E80W20, E100W0 and Degussa P25 TiO_2.

Fig. 12: Plot of DOC verses particle size for various photocatalysts following 6 hours reaction time.

Description of Invention

As discussed hereinbefore, it has been surprisingly found that a composition comprising TiO_2 nanocrystals in the form of agglomerates and/or aggregates; and an anionic species

associated with the TiO_2 agglomerates/aggregates, wherein the diameter of the TiO_2 agglomerates/aggregates is from 0.02 μm to 5.0 μm; the diameter of the TiO_2 nanocrystals is from 4 to 70 nm; and the BET surface area of the composition is from 6 to 250 g/m^2, results in photocatalysts with particularly good properties. Preferably, the introduction of the anionic species is born as a by-product of the method of manufacture of the nanocrystals.

When used herein, the term "primary particles", refers to individual crystals that may or may not associate together form secondary particles. "Secondary particles", when referred to herein are either agglomerates (particles that are physically-bound together; rigidly) or aggregates (particles that are chemically or sinter-bound together; loosely). When used herein, the term "associated" may refer to any type of bonding, such as covalent bonding, Van der Waals attraction or, more particularly, ionic bonding.

When used herein "substantially" refers to the situation where all or almost all of a composition (or component thereof) is in a single form, though minor impurities and/or minor amounts (e.g. less than 1 wt%) of another form (or forms) may exist.

When used herein, the term "comprising" (an open-ended term) is intended to cover the terms "consists of" or "consists essentially of" or equivalents of such phrases (closed terms). This specification explicitly contemplates the situation where the term "comprising" can be replaced by the terms "consists of" or "consists essentially of" or equivalents of such phrases or *vice-versa*. That is, any open-ended term may be replaced by a closed term or *vice-versa*.

When used herein, the term "optionally" refers to a feature that may be present, but can be removed.

In the disclosed compositions the direct band gap of the TiO_2 nanocrystals can be from 3.00 to 3.70 eV (e.g. 3.34 to 3.50 eV) and/or the indirect band gap of the TiO_2 nanocrystals may be from 2.90 to 3.50 eV (3.17 to 3.30 eV). For example, the direct band gap of the TiO_2 nanocrystals may be from 3.35 to 3.45 eV and/or the indirect band gap of the TiO_2 nanocrystals is from 3.20 to 3.26 eV.

While the TiO_2 nanocrystalline compositions may contain different crystalline forms, it is preferred that the TiO_2 nanocrystalline compositions are substantially in the anatase form. For example, the TiO_2 nanocrystalline compositions are entirely in the anatase form, though

said form may contain defects associated with the presence of the anionic species, and the TiO_2 nanocrystals may also form secondary particles (e.g. agglomerates and/or aggregates).

The TiO_2 nanocrystalline compositions may contain an anionic species selected from one or more of the group consisting of SO_4^{2-}, Cl^-, F^-, Br^-, I^-, PO_4^{3-}, NO_3^-, BO_3^{3-}, and SiO_3^{2-}. Preferably, the anionic species is SO_4^{2-}. In certain embodiments, the anionic species may be added during the reaction to generate the TiO_2 nanocrystals or, more particularly, may be present in the material used to generate the same. In certain embodiments, the anionic species may be a mixture of two or more species. When this is the case, both of the species may be added during the hydrolysis reaction to generate the TiO_2 nanocrystals, or one of the anionic species may be present in the material used to generate said TiO_2 nanocrystals, while the others may be added to the hydrolysis reaction.

When the anionic species is SO_4^{2-}, Ti may be present in an amount of from 50.9 wt% to 63.9 wt%, O may be present in an amount of from 36.09 wt% to 44.5 wt%, and S may be present in an amount of from 0.01 wt% to 4.6 wt%. For example, Ti may be present in an amount of from 55.9 wt% to 59.49 wt%, O may be present in an amount of from 40.5 wt% to 41.5 wt%, and S may be present in an amount of from 0.01 wt% to 2.6 wt%, such as Ti may be present in an amount of from 55.9 wt% to 59.0 wt%, O may be present in an amount of from 40.5 wt% to 41.5 wt%, and S may be present in an amount of from 0.5 wt% to 2.6 wt%, or Ti may be present in an amount of from 57.3 wt% to 58.5 wt%, O may be present in an amount of from 40.5 wt% to 40.9 wt%, and S may be present in an amount of from 1.0 wt% to 1.8 wt%. Additionally or alternatively, when the anionic species is SO_4^{2-}, the composition may have FTIR peaks at approximately 3620-3850 cm^{-1}, 3159 cm^{-1}, 1400 cm^{-1}, 1215 cm^{-1}, 1148 cm^{-1}, 1051 cm^{-1} and 980 cm^{-1}.

In certain embodiments, the proportion of Ti-OH species compared to $Ti\text{-}OSO_3$ species of the surface of the aggregates/agglomerates, as measured using the Ti $2p_{3/2}$ peaks using X-ray photoelectron spectroscopy, is from 1.5:1 to 2:1. This may also be expressed with reference to the content of O or S within the composition, as described in the summary of the invention.

In certain embodiments, the diameter of the secondary particles in the composition, (i.e. the agglomerates/aggregates) may be from 0.02 µm to 3.0 µm (e.g. 0.05 µm to 3.0 µm), such as from 0.05 µm to 2.0 µm, such as from 0.1 µm to 1.0 µm. Additionally or alternatively, the

diameter of the TiO_2 nanocrystals (i.e. the primary particles) may be from 5 to 50 nm (e.g. from 5 to 30 nm, from 9 to 26 nm or from 5.7 to 6.4 nm).

In certain embodiments, the BET surface area of the composition may be from 6 to 170 g/m^2, such as from 6.0 to 9.0 g/m^2, or from 20.0 to 90.0 g/m^2 or from 115 to 250 g/m^2 (e.g. from 6.5 to 7.0 g/m^2, or may be from 30.0 to 70.0 g/m^2 or from 145 to 170 g/m^2). While it would be generally expected that a composition with a high surface area may result in better catalytic activity, it has surprisingly been found that the compositions of the current invention may have a relatively low surface area as compared to Degussa P-25 and yet retain a catalytic activity that is many times higher than said catalyst.

While not wishing to be bound by theory, it is suspected that the unexpectedly good catalytic activity of the current compounds may be associated with the presence of a relatively high proportion of Ti-OH and anionic species on the surface of the secondary particles (e.g. as measured by FTIR and/or XPS). In certain embodiments, (e.g. in embodiments where the composition has a BET surface area of from 6.5 to 7.0 g/m^2), the ratio of the anionic species on the surface of the TiO_2 agglomerates/aggregates compared to the anionic species within the interior volume of the TiO_2 agglomerates/aggregates is from 1.5:1 to 30:1, optionally from 2:1 to 10:1, such as from 3:1 to 8:1 (e.g. from 5:1 to 8:1).

In certain embodiments, 0.1 wt% of the composition can reduce the dissolved organic carbon in 99.9 wt% of reverse osmosis concentrate by from 70% to 80% after 6 hours of photocatalytic reaction.

The compositions described herein before may be prepared using a method comprising the steps of:

(a) hydrolysing a titanium source in a water/solvent mixture to form a hydrous TiO_2 material;

(b) filtering the hydrous TiO_2 material and washing the filtered hydrous TiO_2 material with a washing solution;

(c) drying and grinding the filtered and washed hydrous TiO_2 material into a powder; and

(d) calcinating the powder to form anhydrous TiO_2 nanocrystals.

It is intended that steps (a) to (d) be run consecutively. In addition, the anhydrous TiO_2 nanocrystals obtained in step (d) may be optionally subjected to further grinding.

The titanium source may be one or more of the group selected from $TiCl_3$, $TiCl_4$, oxalotitanic acid, titanium ethoxide, titanium n-propoxide, titanium isopropoxide, and titanium n-butoxide or, more particularly, titanyl sulfate,.

The hydrolysis step may be conducted at a temperature of from 25 to 190°C, such as from 85 to 95°C or from 100 to 190°C. The temperature chosen will depend on the titanium source and composition of the water/solvent mixture. Said solvent may be selected from one or more of methanol, ethanol, n-propanol, isopropanol, acetone, acetylacetone, methyl ethyl ketone, methyl propyl ketone, methyl isobutyl ketone, methyl pentyl ketone, butyrolactone, methyl formate, ethyl formate, propyl formate, butyl formate, methyl acetate, oxaloacetate, ethyl acetate, propyl acetate, butyl acetate, and dibasic ester (e.g. ethanol). In certain embodiments, a water/solvent ratio of from 1:10 to 20:1 may be used (e.g. from 2:1 to 4:1). However, it is possible to obtain compositions of the current invention through the use of water alone (i.e. no solvent is present).

In certain embodiments, the weight ratio of the titanium source to the solvent/water in the hydrolysis step is from 1:1000 to 10:1, such as from 1:100 to 1:10.

The washing step may be conducted at ambient temperature. In certain embodiments, the washing solution used in the washing step can be selected from one or more of 0.01 to 5 M ammonia (aq), methanol, ethanol, isopropanol, acetone, methyl ethyl ketone, methyl isobutyl ketone, methyl formate, ethyl formate, methyl acetate, and ethyl acetate (e.g. 0.1 M ammonia (aq)). It will be appreciated that the filtering of the hydrolysed material may occur before and/or after the washing step. Following the washing step, the resulting hydrous TiO_2 material may be dried at a temperature of from 10°C to 100°C for a period of from 0.5 to 24 hours, such as at a temperature of from 40°C to 80°C for a period of from 6 to 12 hours.

In certain embodiments, the calcination step is conducted at a temperature of from 100°C to 1000°C using a temperature ramp of from 0.1°C to 100°C per minute for from 0.1 to 48 hours, such as at a temperature of from 250°C to 600°C using a temperature ramp of from 5°C to 15°C per minute (e.g. 10°C per minute) for from 0.5 to 4 hours (e.g. 400°C or 600°C).

As discussed hereinbefore, while the titanium source may provide an anionic species that becomes associated with the resulting TiO_2 nanocrystals as a by-product. However, for certain titanium sources, the anionic species present may not survive the calcination process,

given this, an anionic source may be added to the titanium source and water/solvent mixture. In certain embodiments, the anionic source may be added to the titanium source and water/solvent mixture even where the titanium source contains an anionic species that would survive the calcination process. In certain embodiments, the anionic source contains one or more (or is capable of producing one or more) anions selected from the group consisting of F^-, Br^-, I^-, PO_4^{3-}, NO_3^-, BO_3^{3-}, and SiO_3^{2-}.

It will be appreciated that any composition formed by the process described hereinbefore is intended to form part of the current invention. In addition, the compositions and products obtained by the processes described hereinbefore are suitable for use as photocatalysts, for example, in the treatment of any one of wastewater, drinking water and ROC, in air purification, and in surface self-cleaning.

EXAMPLES

Materials

Ethanol (95%, Reagent grade), absolute ethanol (99.9%, AR grade), ammonia 25% (AR grade) was purchased from Sigma-Aldrich Singapore Pte Ltd. Deionized (DI) water was generated from Millipore Milli Q Integral 15 system with 0.22 μm filter. This DI water is type I water with resistivity > 18 MΩ·cm and each metal < 1 ppb. Thermocouple temperature controller used in catalyst synthesis is Heidolph EKT 3001. The UV lamp used in photocatalytic reaction is a Blak-Ray B-100AP/R high intensity mercury 100W 365 nm UV lamp from UVP LLC Company. Reverse osmosis concentrate (ROC) with a dissolved organic carbon (DOC) of 24.5 ppm was obtained from Singapore Public Utilities Board (Singapore PUB) water treatment plant. Physical properties of ROC are listed in Table 1.

Parameters	Values
DOC (mg/L)	25.0 ± 2.0
TKN (mg/L)	10 ± 3
COD (mg/L)	60.0 ± 5
pH value	6.9 ± 0.2
Color (Pt-Co)[a]	144 ± 10
Turbidity (ntu)	3.2 ± 0.4
TDS (mg/L)	1129 ± 40
Conductivity (μs/cm)	1705 ± 21
Cations (mg/L)	
Na^+	203 ± 10
Mg^{2+}	7 ± 0.1
K^+	62 ± 5

Parameters	Values
Ca^{2+}	65 ± 8
Anions (mg/L)	
Cl-	256± 16
SO_4^{2-}	217 ± 4
NO_3^-	91 ± 4
NO_2^-	2 ± 1
PO_4^{3-}	39 ± 7

[a] Color was measured in Pt-Co units according to ASTM D1209 "standard test methods for colour of clear liquids (platinum-cobalt scale)".

Table 1

General Analysis

The S and Ti content in the catalysts were measured by EDS and also calculated from XPS. Catalysts surface areas were measured by N_2 adsorption/desorption. Catalyst's crystal phases and sizes were measured by XRD. The morphologies of the catalysts were visualized by SEM and TEM. Semiconductor SO_4^{2-}/TiO_2 band gaps were measured by UV-Vis DRS. Chemical bonding between sulfate and Ti(IV) were confirmed by FT-IR. Catalyst surface compositions and Ti, O, S species were measured by XPS.

Catalyst characterizations

Liquid chromatography – quadrupole time of flight (LCQToF) tandem mass spectrometry with AB Sciex QTOF 5600 MS/MS system and Dionex ULTIMATE 3000 HPLC system was used for separation and identification of organic contaminants in RO concentrate. LC column used is a Waters XTerra MSC18 5.0 µm, 3.9 mm x 150 mm column. Mobile phase A: 0.1% formic acid in DI water; mobile phase B: 0.1% formic acid in methanol. A typical gradient is: 0 minute, 30% B; 4 minute, 70% B; 6 minutes, 30% B.

Shimadzu TOC-Vws total organic carbon analyzer was used to analyze the dissolved organic carbons (DOC). For DOC measurement, samples were diluted 100 or 50 times with ultrapure water. Ultrapure water was measured for DOC and samples' DOC were calculated based on dilution ratio and ultrapure water DOC. DOC calibration standards are 10, 20, 50, 100, 150, 200, 250, 300 and 400 ppb DOC. DOC calibration curve has a good regression linearity R^2 0.9995. Gilden Photonics fluoroSENS fluorescence spectrometer was used to monitor the presence and concentration of humic substances: excitation wavelength 349nm,

emission wavelength scanning range 370 – 700 nm. For VOCs analysis, Shimadzu GCMS-QP2100 plus mass detector was used. UV-Visible spectrum was done on Hach DR 5000 UV-Vis spectroscopy, wavelength 200 – 800 nm.

A similar technique was used to determine the total organics concentration for the samples. A Shimadzu TOC-VWS Total Organic Carbon Analyzer was used to analyze DOC concentration. Inorganic carbon was removed in the TOC analyzer system before analysis by acidification and N_2 purging. Samples were filtered through 0.45 μm Minisart filters prior to analysis. DOC included larger (MW > 2000 Da) and smaller (MW < 2000 Da) molecules. During the DOC measurement, dissolved organic molecules was oxidized by sodium persulfate and phosphoric acid in an 80 °C reaction cell with the assistance of UV irradiation to carbon dioxide detected and quantified by a IR detector.

The textural properties of the catalysts were determined by nitrogen adsorption/desorption (Micromeritics ASAP 2000) at liquid nitrogen temperature. Prior to measurement, each sample was degassed under vacuum at 110°C for 10-20 hours until vacuum is maintained at 5 μBar for more than 10 seconds when vacuum pump was disconnected from sample.

Powder X-ray diffraction (XRD) was measured for crystal phase information with a Siemens D5005 diffractometer equipped with variable slits and a copper anode (Cu Ka X-ray, λ = 1.54056 Å, 40 kV, 40 mA). The diffractograms were recorded over a 2θ range from 15 to 75°. Microstructures of the catalysts were examined by field emission scanning electron microscopy (SEM, JEOL JSM-6701F) at an acceleration voltage of 5.0 kV. Energy dispersive X-ray spectra were done on field emission scanning electron microscopy (FESEM, JEOL JSM-6701F) at an acceleration voltage of 15 kV. Nanostructures of the catalysts were also examined by transmission electron microscopy (TEM, JEOL 3010) operated at 200 kV. The finely grinded sample was suspended in 2-propanol, and one drop of the suspension was placed onto a carbon-coated copper grid and dried before TEM measurements.

For catalyst band gap measurement, UV-Vis DRS diffuse reflectance spectra of powder samples were recorded on Shimadzu 2450 diffuse reflectance UV-Visible spectrophotometer.

FTIR spectrum was carried out using Shimadzu IR Prestige 21. FTIR samples were pre-treated at 80 °C for 8 hours to get rid of adsorbed moisture. KBr was baked at 130 °C for 24 hours. KBr pellet was done on Shimadzu KBr pellet press equipped with a vacuum pump. The powder sample was vacuumed for 5 minutes and then pressed at 78.5 kg pressure with

continuous vacuum for 15 minutes. Sample concentration in KBr powder is 0.5-1%wt. Background spectrum was recorded on pure KBr pellet in air at room temperature 25 °C and was subtracted from the sample spectrum at the same temperature. The IR spectra were recorded by accumulating 32 scans at a spectral resolution of 4 cm^{-1}.

X-ray photoelectron spectrum measurement (XPS) was carried out using Omicron analyser EA125 7-channel spectrometer. The radiation source was monochromatic Mg Kα radiation operating at a power of 300 W (15 kV, 20 mA). Analysis chamber vacuum pressure is 4.3×10^{-9} Torr. Samples were prevacuumed for overnight to ensure adsorbed species were removed. During measurement, constant analyser energy modes (CAE) for wide scan and elemental scan were 50 eV (bigger slit) and 20 eV (smaller slit), respectively. Emission angle is 15°.

Equipment work function Φspec = 4.42 eV. Curve fitting was done on software XPSPEAK41. Linear background was used for fitting. Position constrains and area constrains were used. Ti and S 2p photoelectrons split into 2 peaks $2p_{3/2}$ and $2p_{1/2}$ due to spin orbit coupling. For Ti species, position constrains used is 5.6 eV (binding energy of $2p_{1/2}$ is 5.6 eV higher than that of $2p_{3/2}$), and area constrains used is 50% ($2p_{1/2}$ is 50% area of $2p_{3/2}$). For S species, position constrains used are 1.18 eV, and area constrains used are 50%. For O species, no constrains are needed. $\Sigma\chi^2$ was used to monitor the wellness of peak fitting, the lower the better. Referring to the standard chisquared χ^2 distribution table, with the peaks' degree of freedom the possibility whether fitted curves are same original peaks could be found at the table.

General Procedures

1. Preparation of Catalysts

4 grams (16 mmol) of titanyl sulfate ($TiOSO_4 \cdot xH_2O$) was added to a 100 mL ethanol/water mixture (see Samples for ratio), with stirring to dissolve. After dissolution, the mixture was heated to 85-95°C until a white precipitate was generated. After the titanyl sulfate was fully hydrolyzed, the mixture was filtered or centrifuged, and the white precipitate was washed with a mixture of 0.1M ammonia and ethanol, and subsequently filtered or centrifuged again. The white precipitate was dried at 40-70 °C in an oven overnight and ground into a powder,

followed by calcination at 400 °C for 1 hour, followed by and further grinding to form a fine powder.

2. *Photocatalytic Reactions*

Photo-catalytic reactions of reverse osmosis concentrate (ROC) were done with 0.1%wt catalysts SO_4^{2-}/TiO_2 in a quartz reactor with temperature control 25 +/- 0.2 °C and UV lamp 365 nm wavelength (100 W) irradiation. UV lamp was 7 cm away from the ROC surface with a light intensity 18 ± 0.1 mW/cm^2 (Fig. 1). Reaction time varies from 1 to 24 hours. Dissolved organic carbon (DOC) was measured to indicate all organics in ROC. Photo-catalytic conversion of organics in ROC was calculated from measured DOC before and after reaction. Humic substances' degradation in ROC was monitored by fluorescence emission spectra.

Example 1

Catalysts were prepared using General Procedure 1, using the ratios of ethanol:water (E:W) listed below in Table 2. For catalyst designation, E means ethanol, the number behind E means the percentage of ethanol in the mixture of ethanol/water, W means water, the number behind W means the water percentage in the mixture of ethanol/water; e.g., E33W67 indicates the catalysts were prepared from a mixture of 33%v/v ethanol and 67%v/v water. SO_4^{2-}/TiO_2 catalysts were named as E100W0, E80W20, E67W33, E50W50, E33W67, E20W80 and E0W100 according to their ethanol/water percentage 100/0, 80/20, 67/33, 50/50, 33/67, 20/80 and 0/100, respectively. Alternatively, the catalysts may be referred to by the designations provided in Table 2 below. A further catalyst was prepared (101212B), which is identical to E20W80, except that it was subjected to calcination for 4 hours at 400 °C, instead of for 1 hour and its activity is shown in Figure 2 (as discussed below).

Catalyst	#1 (E0W100; 281212A)	#2 (E20W80 201212A)	#3 (E33W67 111212A)	#4 (E50W50 121212A)	#5 (E67W33 141212A)	#6 (E80W20 201212B)	#7 (E100W0 241212A)
E:W Ratio	0:5	1:4	1:2	1:1	2:1	4:1	5:0
Dissolution time (hrs)	0.25	0.25	2.5	3.5	6	12	2 days not fully dissolved

Table 2

Example 2

Each of the catalysts listed in Table 2 were subjected to the photocatalytic reaction with ROC as described in General Procedure 2, as was the photocatalyst Degussa P-25. The reactions were run for from 6 hours up to 24 hours (as discussed below) and analysis of the reaction mixtures were conducted on an hourly basis.

Figure 2 shows the reduction in total organic concentration in ROC over a 6 hour period for these catalysts, while Figure 3 shows the reduction in total organic concentration over a 24 hour period for catalyst #3 when used to treat ROC.

According to the analysis by LC-QToF and fluorescence spectroscopy, organics in original ROC include humic substances 23.35 ppm (95.30%wt), surfactants 1.06 ppm (4.33%wt) and drug residues 0.09 ppm (0.37%wt). Fig. 4a shows the conversion of organics in ROC (C/C_0) based on dissolved organic carbon (DOC) for Degussa P25 and the $SO4^{2-}/TiO_2$ catalysts of Table 1 after 6 hours of photocatalytic reaction. When the percentage of ethanol used during synthesis is less than 40%v/v, SO_4^{2-}/TiO_2 catalysts (E0W100, E20W80 and E33W67) have higher photocatalytic activity than Degussa P25. The best photocatalytic activity was achieved for catalyst E20W80, with a conversion of 76.8%, which is much higher than that of Degussa P25 (41.1% after 6 hours reaction time). Catalysts E0W100 and E33W67 are only slightly less active than E20W80, but are still much more active than Degussa P25. However, when the ethanol percentage is more than 40% v/v, the photocatalytic activity of the SO_4^{2-}/TiO_2 catalysts (E50W50, E67W33, E80W20, E100W0) decreases to < 11% DOC conversion after 6 hours UV irradiation, so are not as good as Degussa P25.

Organics in ROC were separated and identified using LC-QToF tandem mass spectroscopy. Besides humic substances, which were monitored by fluorescence spectrometry, 75 organic compounds were identified and their molecular structures were deduced. 67 Compounds are surfactants most likely from detergents. These surfactants are very difficult to degrade under UV/TiO_2, almost no degradation happened after 24 hours photocatalytic reaction over all the catalysts. 8 Compounds are likely drug residues. 5 Drug residues were degraded for 24 hours' photocatalytic reaction over SO_4^{2-}/TiO_2 catalyst E20W80 with a conversion 80.6%, while the other 3 drug residues were 100% degraded after 6 hours.

UV-vis spectrum absorbance at 254 nm wavelength was also used to monitor the organic compounds with conjugated double bonds. Energy of 254 nm UV light matches with the

orbital energy difference of conjugated π bond and π* anti-bond, so conjugated π bonds (such as humic acids) absorb 254 nm UV light. Figure 4c shows normalised UV-Vis absorbance at 254 nm after ROC 6 hours photocatalytic reaction over different catalysts. As shown in Figure 4c, after 6 hours of reaction time, the absorbance at 254 nm (A254) is much lower for E0W100, E20W80 and E33W67 than for Degussa P25, while E50W50, E67W33, E80W20, E100W0 have higher absorbances. As increasing conjugation leads to a change in absorbance (e.g. the absorbance peak for lycopene is around 450~530 nm) similar UV absorbance spectra were taken after 6 hours of reaction time at 455 nm (Figure 4d), which shows the same pattern of absorbance. These results indicate that E0W100, E20W80 and E33W67 are better than Degussa P25, while E50W50, E67W33, E80W20, E100W0 are worse.

Humic substances mainly include humic acid and fulvic acid. Humic acids (HAs) are organic macromolecules, formed during degradation of plants and microbial materials with a high molecular weight (5000 – hundreds of thousands of Daltons). Tentatively, the structure is a flexible network of aromatic chains bonded by long alkyl chains, also containing oxygen-rich functionalities, such as carbonyl, carboxylic, methoxyl, hydroxyl, phenol, and quinoid groups. The origin of and the age of humic substances affect the HAs molecular structure, molar mass, and organic functional groups. Photocatalytic degradation occurs *via* the production of low molecular-weight organic carboxylic acids (4-hydroxybenzoic acid, oxalic acid, succinic acid, and malonic acids) as reaction intermediates to final oxidation products - water and CO_2. The use of fluorescence spectroscopy has been used for the characterization of humic substances. Recently, excitation-emission matrix (EEM) spectroscopy was developed to quantify the fluorescence species. A ROC excitation wavelength scan showed the strongest excitation wavelength at 349 nm. An emission scan from 370 to 700 nm was carried out when excitation wavelength was 349 nm. Rayleigh scattering peak was avoided in the spectrum by a wavelength distance of 21 nm between emission scan starting point (longer wavelength) and excitation wavelength. ROC emission peak is 430 nm, while for degraded samples after photoreaction, the peak wavelengths vary between 410 and 435 nm. Integration areas from 370 to 700 nm were used to calculate the conversion percentage of humic substances. Photocatalytic degradation of humic substances over SO_4^{2-}/TiO_2 catalyst E33W67 (Ethanol 33%, Water 67% during preparation) is a first order reaction. In Fig. 4b $\ln(C_0/C)$ (based on fluorescence integration area) is plotted versus reaction time as a linear line. C_0 is the original ROC concentration, C is the degraded ROC concentration after photoreaction over SO_4^{2-}/TiO_2 catalyst E33W67. Humic substances photocatalytically degrade to CO_2, H_2O, nitrate, nitrite and ammonium ions (Equation (A)). The Langmuir-

Hinshelwood (L-H) law has been widely used in liquid-gas-phase photocatalysis. This law successfully explains the kinetics of reactions that occur between two adsorbed species, a free radical and an adsorbed substrate, or a surface bound radical and a free substrate. The initial rate of substrate removal (*r*) varies proportionally with the surface coverage (θ), as shown in equation (B), apparent rate constant (*k'*) can be obtained from the slope of the linear regression analysis of the $\ln(C_0/C) \sim t$ plot as 0.62744 h^{-1} according to equation (C).

Humic Substances $\longrightarrow$ $CO_2 + H_2O + NO_3^- + NO_2^- + NH_4^+$ (A)

$$r = -\frac{dC}{dt} = k\theta = \frac{kKC_0}{1+K\,C_0} \qquad (B)$$

$$\ln\left(\frac{C_0}{C}\right) = k't \qquad (C)$$

$$k' = k \times K \qquad (D)$$

Where C_0 is the initial concentration of the organic substrate S; t is the reaction time; k is the Langmuir adsorption constant of S; K is the adsorption equilibrium constant which is a measure of the intrinsic reactivity of the photoactive surface S. k' is apparent rate constant (equation (D)).

Example 3

Characterisation of Catalysts

X-Ray Powder Diffraction

Powder X-ray diffraction patterns of SO_4^{2-}/TiO_2 catalysts E0W100, E20W80, E33W67, E50W50, E67W33, E80W20 and E100W0 showed that their crystal phases are anatase with primary particles in nano-sizes (Figure 5). Their 5 anatase peaks belong to planes (101), (103)+(004)+(112), (200), (105)+(211), and (118) at 2θ angle 25.4, 38.0 , 48.1,54.7, and 62.9°. Degussa P25 was a mixture of anatase and rutile phases as primary particles where the anatase peaks belong to planes (101), (103), (004), (112), (200), (105), (211), and (118) at 2θ angle 25.4, 37.1, 38.0, 38.7, 48.1, 54.1, 55.1 and 62.9°. The 6 rutile Degussa P25 peak belong to planes (110), (101), (111), (211), (220), and (301) at 2θ angle 27.5, 36.2,

40.7, 54.5, 56.8, and 69.0°. For nano-size powder, XRD peaks broaden. The Degussa P25 anatase and rutile ratio is calculated according to peak area ratio of anatase major peak (101) and rutile major peak (110) and response factor 0.884 (equation (1)).

$$Rutile(\%) = \frac{1}{0.884 \times \frac{A}{R} + 1} \times 100\% \qquad (1)$$

A – anatase major plane (101) peak area; R – rutile major plane (110) peak area. Degussa P25 calculated anatase and rutile phases are 77.4%wt and 22.6%wt. Micron size (μm) particles' scattered X-rays interfere and cancel each other only intensified at Bragg's angle, while nanoparticles too small to have enough plane interference to cancel each other at slightly bigger or smaller than Bragg's angle, causing peak broadening.

Peak broadening can be used to calculate the average sizes of nano-phases using Scherrer's formula (equation (2)) when the sizes are below 100 nm.

$$\text{Scherrer's formula} \qquad t = \frac{K \times \lambda}{B \times \cos \theta_B} \qquad (2)$$

t – thickness of crystalline (diameter); K – constant depends on crystal shape (0.89); λ - X-ray wavelength 1.5406 Å for Al Kα; B – full width at half maximum (FWHM); θ_B – Bragg angle.

Calculated sizes are summarized in Table 3. Anatase and rutile lattices are tetragonal and primitive tetragonal, respectively and with Z = 4 and 2 in a unit cell, respectively. SO_4^{2-}/TiO_2 catalysts E0W100, E20W80, E33W67, E50W50, E67W33, E80W20 and E100W0 average crystalline sizes are within 4 ~ 7 nm, smaller than Degussa P25 anatase and rutile particles average sizes 23.7 and 36.8 nm, respectively. Lattice parameters a and c are calculated based on the d-spacing according to equation (3) for a tetragonal crystal system.

$$\text{Tetragonal} \qquad \frac{1}{d^2} = \frac{h^2 + k^2}{a^2} + \frac{l^2}{c^2} \qquad (3)$$

For calculation of a and c of anatase major peak lattice plane (101) and second intense peak lattice plane (200) are used, while for rutile major peak lattice place (110) and third intense peak lattice plane (101) were chosen because its second intense plane (211) has some

overlaps with anatase plane (105) and (211). Results of a and c are listed in Table 3. Anatase lattice unit cell volume ($V = a^2 \cdot c$) is bigger than that of rutile.

Catalyst\ Parameters	#6	#5	#4	#3	#2	#1	Degussa P25 Anatase	Degussa P25 Rutile
B(°) (101)[a]	1.67	1.60	1.43	1.28	1.26	1.41	0.34	0.22
B(rad)	0.02913	0.02791	0.02495	0.02233	0.02198	0.02460	0.00593	0.00384
$2\theta_B$ (°)	25.25	25.53	25.62	25.50	25.05	25.20	25.42	27.52
θ_B (101)[a]	12.63	12.77	12.81	12.75	12.75	12.60	12.71	13.76
$\cos\theta_B$	0.97582	0.97528	0.97511	0.97534	0.97534	0.97592	0.97550	0.97130
t (Å)	48.232	50.370	56.368	62.959	59.700	57.120	236.984	367.829
t (nm) *	4.8232	5.0370	5.6368	6.2959	5.970	5.7120	23.6984	36.7829
$\sin\theta_B$ (101)[a]	0.21857	0.22095	0.22172	0.22070	0.22070	0.21814	0.22002	0.23786
d(101)[a] (Å)	3.5243	3.4863	3.4742	3.4903	3.4903	3.5312	3.5011	3.2385
$2\theta_B$ (°) (200)[b]	48.10	48.10	48.10	48.10	48.10	48.10	48.10	36.15
θ_B (200)[b]	24.05	24.05	24.05	24.05	24.05	24.05	24.05	18.08
$\sin\theta_B$ (200)[b]	0.40753	0.40753	0.40753	0.40753	0.40753	0.40753	0.40753	0.31026
d(200)[b] (Å)	1.8902	1.8902	1.8902	1.8902	1.8902	1.8902	1.8902	2.4827
a (Å)	3.7803	3.7803	3.7803	3.7803	3.7803	3.7803	3.7803	4.5800
c (Å)	9.7428	9.0162	8.8138	9.06867	9.0867	9.8907	9.2825	2.9545

a For rutile phase in Degussa P25, major plane is (110).
b For rutile phase in Degussa P25, third intense plane is (101).
* t = particle size (average diameter).

Table 3

Surface Area of Catalysts

BET Surface areas of photocatalysts SO_4^{2-}/TiO_2 and Degussa P25 TiO2 are listed in Table 4. With higher ethanol ratio (>33%v/v) during synthesis, the resulting photocatalysts SO_4^{2-}/TiO_2 have lower BET surface areas < 20 m^2/g, which is lower than that of Degussa P25 (49.80 m^2/g). With higher water ratio (>80%v/v) during preparation, the resulting photocatalysts SO_4^{2-}/TiO_2 have around 3 times higher BET surface area than that of Degussa P25. Absorbed DOC quantities are also listed in Table 4. Absorbed DOC was the DOC quantity absorbed by photocatalyst from RO concentrate (ROC). 0.05 g Catalyst was placed into 50 ml of ROC for 5 minutes with stirring but without UV light, sample was drawn and centrifuged

to remove catalysts and then sample DOC was measured. The difference between the measured DOC after catalyst adsorption and that of original RO concentrate is the absorbed DOC. BET surface area appears to have a clear correlation with the absorbed DOC except for E33W67 SO_4^{2-}/TiO_2 which has low surface area but high absorbed DOC. Photocatalysts with lower surface areas absorbed lesser DOC from ROC,while more DOC could be absorbed onto photocatalysts with higher surface areas.

Photocatalyst BET surface area also has a clear correlation with photocatalytic activity (Table 4). When the photocatalyst has larger surface area, it has higher photocatalytic activity. The photocatalyst with smaller surface has lower photocatalytic activity except for E33W67 SO_4^{2-}/TiO_2 which has low surface area but high activity.

Surface area, absorbed DOC, DOC conversion and elemental compositions of SO_4^{2-}/TiO_2 Photocatalysts and Degussa P25 TiO_2.

Properties	E100W0	E80W20	E67W33	E50W50	E33W67	E20W80	E0W100	Degussa P25
BET surface area (m^2/g)	2.22	2.86	1.40	17.80	6.67	146.90	165.10	49.80
Absorbed DOC (ppb) [a]	1.43	0.67	1.30	0.02	3.35	3.33	2.46	2.71
DOC conversion (%)	9.95	3.75	10.76	4.40	72.89	76.80	75.30	41.17
Ti content (%wt) [b]	45.64	56.29	55.45	56.12	57.38	58.37	58.45	59.95
O content (%wt) [b]	44.80	41.26	41.54	41.32	40.90	40.57	40.55	40.05
S content (%wt) [b]	9.56	2.45	3.00	2.56	1.72	1.06	1.00	0.00

a Absorbed DOC was the DOC quantity absorbed by photocatalyst from RO concentrate. 0.05 g Catalyst was placed into 50 ml of RO concentrate for 5 minutes with stirring but without UV light, sample was drawn and centrifuged to remove catalysts and then sample DOC was measured. The difference between the measured DOC after catalyst adsorption and that of original RO concentrate is the absorbed DOC.

b Elemental composition data is from energy dispersive spectroscopy (EDS).

Table 4

Analysis by EDS

The elemental content of the SO_4^{2-}/TiO_2 photocatalysts was measured by energy dispersive X-ray spectroscopy (EDS). EDS spectra of E20W80 and E80W20 are shown in Fig 6a and 6b, confirming the existence of sulfur in the SO_4^{2-}/TiO_2 photocatalysts, but not in Degussa P25. When the percentage of ethanol is higher during synthesis, the resulting SO_4^{2-}/TiO_2 photocatalysts have higher S content. The S content is from the sulfate in the TiO_2 precursor. When the ethanol ratio is higher, water is less, so the relative precursor concentration in water is higher although the overall amount is fixed (4%wt TiO_2 precursor in ethanol/water mixture), resulting in a higher S content in the photocatalyst. The sulfur content in E0W100, E20W80, and E33W67 are relatively low (compared to E50W50, E67W33, E80W20 and

E100W0) - 1.00, 1.06 and 1.72%wt, respectively, but with higher photocatalytic activity DOC conversion 75.3, 76.8, and 72.89%wt, respectively, after 6 hours photocatalytic reaction of ROC, which is higher than that that of Degussa P25 (Table 4). The sulfur content in E50W50, E67W33, E80W20 and E100W0 are relatively higher (compared to E0W100, E20W80, and E33W67) - 2.56, 3.00, 2.45, and 9.95%wt, respectively, with much lower photocatalytic activity DOC conversion 4.40, 10.76, 3.75 and 9.95%wt, respectively.

Chemical Bond Analysis

Chemical bonding information can be extracted from the FT-IR spectra of the compositions. Fig. 7 shows FT-IR spectra of SO_4^{2-}/TiO_2 photocatalysts E20W80, E33W67, E50W50, E67W33, E80W20 and Degussa P25 TiO_2. Chemical bonding structures corresponding to each peak are summarized in Table 5. 3770 (3620 ~ 3850) cm^{-1} is assigned to the Ti(IV)-OH hydroxyl group stretching. 3420 cm^{-1} is assigned to associated –OH stretching, weakly chemisorbed and bridged, hydrogen bonded to Ti(IV)-OH, Ti(IV)-O, Ti(IV). 3159 cm^{-1} is assigned to associated hydroxyl (–OH) stretching, hydrogen bonded with SO_4^{2-} ions. 1636 cm^{-1} is assigned to the δH_2O band, H-O-H bending for H_2O molecule adsorbed on surface. 1400 cm^{-1} is assigned to S=O stretching of SO_4^{2-} ions bonded to Ti(IV)-OH, Ti(IV)-O, Ti(IV). 1215,1148, 1051, and 980 cm-1 are assigned to S-O asymmetric and symmetric stretching, S-O asymmetric and symmetric bending of bonded SO_4^{2-} ions. 760 and 646 cm^{-1} are assigned to asymmetric and symmetric stretching of structural Ti-O-S bonds. 594 and 490 cm^{-1} are assigned to asymmetric and symmetric stretching of structural Ti-O-Ti bonds.

Degussa P25 TiO_2 doesn't show Ti-OH peak at ~3770 cm^{-1} (Fig. 7). E80W20 and E67W33 SO_4^{2-}/TiO_2 also do not have Ti-OH peak at ~ 3770 cm^{-1}. Although all samples were equally heated at 80 °C for 8 hrs, hydrogen-bonded –OH stretching decreases from E0W100 (low ethanol during preparation) to E80W20 (high ethanol percentage during preparation). SO_4^{2-}/TiO_2 photocatalysts E20W80, E33W67, E50W50, E67W33 and E80W20 have peaks at 3159 cm^{-1}, which is associated with hydroxyl –OH stretching, hydrogen bonded with SO_4^{2-} ions. The peak intensity at 3159 cm^{-1} decreases from E0W20 to E80W20. Degussa P25 TiO_2 doesn't have 3159 cm^{-1} peak. 1400, 1215, 1148, 1051, and 980 cm^{-1} peaks get stronger from E0W100 to E80W20. While Degussa P25 TiO_2 doesn't have these 5 peaks, which are related to sulfate ions. From E0W100 to E80W20, Ti-O-Ti structural vibration peaks at 594 and 490 cm^{-1} get weaker but Ti-O-S peak at 760 and 646 cm^{-1} get stronger.

Peak wavenumber (cm^{-1})	Assignment	Peak wavenumber (cm^{-1})	Assignment
3770 (3620 ~ 3850)	Ti(IV)-OH stretching	1051	S-O asymmetric bending of bonded SO_4^{2-} ions
3420	Associated –OH stretching, weakly chemisorbed and bridged, hydrogen bonded to Ti(IV)-OH, Ti(IV)-O, Ti(IV)	980	S-O asymmetric bending of bonded SO_4^{2-} ions
3159	Associated –OH stretching, hydrogen bonded with SO_4^{2-} ions	760	Ti-O-S asymmetric stretching
1636	δH_2O band, H-O-H bending for H_2O molecule adsorbed on surface	646	Ti-O-S symmetric stretching
1400	S=O stretching of SO_4^{2-} ions bonded to Ti(IV)-OH, Ti(IV)-O, Ti(IV)	594	Ti-O-Ti asymmetric stretching
1215	S-O asymmetric stretching of bonded SO_4^{2-} ions	490	Ti-O-Ti symmetric stretching

Peak wavenumber (cm^{-1})	Assignment	Peak wavenumber (cm^{-1})	Assignment
1148	S-O symmetric stretching of bonded SO_4^{2-} ions		

Table 5

Analysis by XPS

X-ray photoelectron spectroscopy (XPS) is an ideal tool for material surface (XPS 3-10 nm depth; EDS 2~3 μm depth) elemental composition and chemical state characterization. XPS samples of SO_4^{2-}/TiO_2 photocatalysts E33W67 and E80W20 were vacuumed overnight to remove adsorbed water molecules. In both samples, Ti 3p, S 2p, S 2s, C 1s, Ti 2p, O 1s, Ti 2s, O (KLL), Ti (LMV) spectrum lines were observed from low to high binding energy (BE) (Fig. 8a). Elemental scans were done for C 1s, Ti 2p, O 1s and S 2p to study the photocatalysts' surface compositions and each element's chemical state, chemical environment, and elemental species' relative atomic ratio. All XPS spectrum peaks' fitting results are summarized in Table 6 (split into Tables 6A and 6B below). Both samples' C 1s spectra show two peaks which are fitted to two peaks meaning two carbon species C^a and C^b exist (Fig. 8b). Carbon could be residue from the ethanol during preparation. C^a BE uncommon at 291.8 eV, C^b BE common at 285.4 eV. C^a 291.8 eV BE is very high, which could be due to neighbouring SO_4^{2-}/TiO_2 ions, as sulfonate is a well-known electron withdrawing group (EWG) in organic chemistry, causing the electron density of carbon C^a to decrease. With lower electron density, BE would be higher due to less shielding from nucleus attraction. C 1s spectrum is usually used to check the BE positions are correct, like an "internal standard". C^b at 285.37 eV confirms the BE are calibrated. C^b could be those carbons bonded to oxygen species. In sample E33W67, the relative percentages of C^a and C^b species are 34.3% and 65.7%, respectively. Sample E80W20 has a higher C^a percentage 46.1%, which implies a higher percentage of SO_4^{2-}, since C^a is related to SO_4^{2-}. This agrees with EDS results (Table 7).

	Binding Energy(eV)					
	C 1s	O 1s	S $2p_{3/2}$	S $2p_{1/2}$	Ti $2p_{3/2}$	Ti $2p_{1/2}$
E33 W67	291.8	538.3	176.2	177.4	465.9	471.5
	285.4	536.6	169.6	170.7	465.3	470.9
		532.8			459.7	465.3
E80W20	291.0	537.4	174.8	176.0	465.0	470.6
	285.6	535.8	170.0	171.2	462.2	467.8
		533.2			459.9	464.9
	FWHM (eV)[a]					
E33 W67		1.98	2.10	1.78	1.22	1.99
		1.85	2.48	5.52	1.92	2.87
		4.64			1.31	5.66
E80W20		2.32	4.23	2.12	2.10	2.46
		1.91	2.43	3.39	3.40	3.44
		3.71			1.57	2.52

	Peak Area							
	Ti $2p_{3/2}$	Ti $2p_{1/2}$	Ti Ratio	S $2p_{3/2}$	S $2p_{1/2}$	S Ratio	O 1s	O ratio
E33 W67	1760.4	880.2	33.8%	640.1	320.0	82.0%	3434.4	30.9%
	3050.6	1052.3	58.6%	140.2	70.1	18.0%	5928.0	53.3%
	391.5	195.8	7.5%				1755.4	15.8%
E80W20	2420.7	1210.4	47.9%	475.5	237.7	57.5%	4329.8	35.7%
	1618.3	809.1	32.0%	351.3	175.7	42.5%	2847.4	23.5%
	1015.3	507.7	20.1%				4949.8	40.8%
	$\sum x^2$ [b]				p-values [e]			
	O 1s	Ti 2p	S 2p	C 1s	O 1s	Ti 2p	S 2p	C 1s
E33 W67	1.231	0.917	0.590	1.519	>0.50	>0.95	>0.90	>0.20
E80W20	1.182	0.827	0.685	0.961	>0.50	>0.95	>0.80	>0.30

Table 6A

	ASF [c]		S/Ti Ratio [d]
	Ti $2p_{3/2}$	S 2p	
E33 W67	1.40	0.70	0.23
E80W20			0.25

Table 6B

a FWHM = full width at half maximum.

b $\Sigma\chi^2$ chi-squared distribution.

c ASF = atomic sensitivity factor.

d S/Ti ratio = S/Ti atomic ratio calculated from peak area and ASF.

e p-Value: probability of observing a test statistic at least as extreme in a chi-squared distribution; when $p > 0.05$,

the difference is not-significant; when $p < 0.05$, the difference is significant.

Ti 2p spectrum (Fig. 8c) was fitted into 3 Ti (IV) species: Ti^a, Ti^b, and Ti^c. Ti (III), which is usually located at 456.0 ± 1.0 eV, was not detected in either sample. Ti 2p spectrum splits into $2p_{3/2}$ and $2p_{1/2}$ due to spin-orbit coupling. $2p_{3/2}$ and $2p_{1/2}$ are 4-fold and 2-fold degeneracies, respectively, resulting peak area ratio 2:1 (4:2). BE of Ti $2p_{3/2}$ is lower than Ti $2p_{1/2}$, the energy difference is the splitting energy (Δ = 5.54 eV). Sample E33W67 $2p_{3/2}$ BEs of Ti species Ti^a, Ti^b, and Ti^c are 465.9, 465.3, and 459.7 eV, with a relative percentage 33.8, 58.6, and 7.5%, respectively. Sample E80W20 $2p_{3/2}$ BEs of Ti species Ti^a, Ti^b, and Ti^c are 465.0, 462.2, and 459.9 eV, with a relative percentage 47.9, 32.0, and 20.1%, respectively. Ti^c at 459.7 (or 459.9 eV) is most common Ti-O species (Fig. 8d). Ti^b and Ti^a are assigned to Ti-OH and Ti-OSO_3 species, respectively (Fig. 8d). The Ti peaks fitting chi-squared x^2 - distribution $\Sigma\ x^2$ is 0.917 and 0.827, respectively, for E33W67 and E80W20 (Table 6). The degree of freedom equals 6 (3 Ti species, each has 2 peaks $2p_{3/2}$ and $2p_{1/2}$), the corresponding p-values (p – probability) can be found from the x^2 – distribution table both > 0.95. p-Value is the probability of observing a test statistic at least as extreme in a chi-squared distribution; when $p > 0.05$, the difference is not-significant; when $p < 0.05$, the difference is significant. In the fitting of Ti peaks, the p values > 0.95, means the difference between fitted and original peaks is not-significant. BE difference of same element's different species are mainly due to the difference of electron density. Electron density sequence Ti^a < Ti^b < and Ti^c (Fig. 8a). In Ti^c species (Ti-O species), oxygen feeds back some σ and π electron cloud into Ti empty 3d orbitals. While in Ti^b species (Ti-OH species, neutral),

oxygen feeds back some σ electron cloud into hydrogen's empty 1s orbital, and therefore less σ and π electron cloud available for Ti empty 3d orbitals. So Ti^b has less electron density than Tia. For Tic species (Ti-OSO_3 species), two oxygen atoms single-bonded to sulfur do not feed σ electron cloud clouds into Ti 3d orbitals due to orientation mismatch and feed less π electron clouds into Ti 3d orbitals due to some bond angle stress between O 2p and Ti 3d orbitals; therefore Ti^c species have even less electron density in 3d orbitals than Tib. With less electron density in 3d orbitals, there is less shielding from nucleus's attraction for 2p electrons, causing 2p photoelectron higher BE. Sample E80W20 has higher Ti^a and less Ti^b species (relative percentage) than E33W67, which indicates more surface sulfate content and less surface hydroxyl –OH groups in sample E80W20. This result agrees with EDS results (Table 7) and FT-IR results (see Example 6).

O 1s spectrum (Fig. 8e) was fitted into 3 oxygen species: O^a, O^b, and O^c. E33W67 and E80W20 oxygen peak fitting both have a p-value > 0.50 (Table 6), implying that the difference between fitted and original peaks is not-significant. Sample E33W67 oxygen species O^a, O^b, and O^c are found at 538.3, 536.6, and 532.8 eV, respectively, and have a relative percentage of 30.3, 53.3 and 15.8%. Sample E80W20 oxygen species O^a, O^b, and O^c are found at at 537.4, 535.8, and 533.2 eV, respectively, have a relative percentage of 35.7, 23.5 and 40.8%, respectively. O^c is assigned to Ti-O species the most common lattice type oxygen in metal oxide. O^b is assigned to Ti-OH species, while O^a is assigned to uncommon oxygen double bonded to sulfur in Ti-OSO3 species (Fig. 8f). Oxygen at high BEs (538.3, 537.4 eV) were not reported for inorganic oxides in literature. In NIST XPS database, over a few hundred oxygen species, besides satellites (much smaller than main peak), a few organic compounds have such high BE: $C_6H_{11}OCH_3$ (537.89 eV), $CH_3CH(OH)CH_3$ (538.51 eV), $(CH_3)_2CHOCH_3$ (538.09 eV), CH_2CHCH_2OH (538.78 eV), $CH_2CHCH_2OCH_2CH_3$ (538.11 eV), C_6H_5OH (539.23 eV), $C_6H_5OCH_3$ (538.70 eV), $CH_3CHCHOCH_2CH_3$ (538.47 eV), $CH_3OC(CH_2)CH_3$ (538.84 eV), $CH_2CHOCH_2CH_3$ (538.72 eV). In our case, the O^a peaks in both samples are as big as relative peak area 30.3 and 35.7%, respectively. So O^a species are not satellites. The above a few organic compounds have high BEs for oxygen due to less electron densities on oxygen caused by covalent bonds, instead of ionic bonds in inorganic oxides. Sample E33W67 and E80W20 oxygen species O^a high BEs have strong organic oxygen characteristics, so O^a is not likely pure inorganic oxygen species, but more like an organic oxygen species. And O^a percentage (XPS) increases with higher S content (EDS). Therefore, we propose O^a to be assigned to oxygen double bonded (covalent bonds) to sulfur in Ti-OSO_3 species (Fig. 8f), like sulfonate

groups. The assignment of 3 oxygen species can also be determined and explained by their electron density models. As shown in Fig. 8b, O^c (Ti-O) has 8 electrons in its 2s and 2p orbitals, with little electron cloud feeds to empty Ti 3d orbitals due to ionic bonding between Ti and O^c, resulting O^c has more electron density. O^b also has 8 electrons in its 2s and 2p orbitals, with little electron cloud feeds to empty Ti 3d orbitals, but some electron cloud feeds to hydrogen 1s orbital due to formation of a weak covalent bond between O and H, resulting O^b electron density < O^c. Note that hydrogen electronegetivity is as low as 2.2, the weak covalent bond between H and O in O^b species does not draw much electron cloud away from O. In O^a species (Ti-OSO_3), there are 2 electrons in between O and S forming a strong covalent double bond S=O. Note that S has higher electronegativity 2.58 (attracts electron stronger) and high positive charge +6 (strong electrostatic interaction), sulfur draws almost 1 electron away from oxygen through the strong covalent bond, resulting less electron density on Oa than Ob. So electron density sequence $O^a < O^b < O^c$, which results in corresponding BE sequence $O^a > O^b > O^c$ due to less shielding to nucleus's attraction from less electron density. Sample E80W20 has more O^a percentage and less O^b percentage than E33W67, which means more S content and less hydroxyl –OH groups in E80W20. This is consistent with Ti 2p XPS results (Fig. 8c, Table 6), EDS results (Table 7) and FT-IR results.

S 2p spectrum (Fig. 8g) was fitted into 2 sulfur species S^a and S^b at BE 176.2 and 169.6 eV for sample E33W67, at BE 174.8 and 170.0 eV for sample E80W20. As shown in Fig. 8h, S^a is assigned to bridged bidentate sulfate species Ti-O(O=S=O)O-Ti, while S^b is assigned to chelating bidentate sulfate species Ti-OO(O=S=O). S^a has less electron density than S^b. In S^b species Ti-OO(O=S=O) chelating bidentate sulfate, two oxygen ions single-bonded to S feed little π electron cloud into one Ti 3d empty orbitals due to orientation mismatch resulting from bond angle stress between O 2p orbital and Ti 3d orbitals (Fig. 8c). Therefore, these two oxygen ions single-bonded to sulfur have more electron cloud "reserved" for the S, resulting in more electron density in S^b species. In S^a species bridged bidentate sulfate species Ti-O(O = S =O)O-Ti, two oxygen ions single-bonded to S feed some σ electron cloud and more π electron cloud to two Ti 3d orbitals with the match orientation between O 2p orbitals and Ti 3d orbitals due to less bond angle stress (Fig. 8c). Therefore, these two oxygen ions which are single bonded to sulfur have less electron cloud "left" for the S, causing less electron density in S^a species. Sample E80W20 has more S^b species (one S links to one Ti through O) and less S^a species (one S links to two Ti through O) than those of sample E33W67, means more sulfate in sample E80W20. Sulfur XPS results align well with Ti, O, C XPS data, EDS and FT-IR data.

Catalyst	S/Ti atomic ratio		S content* (% wt)	SA** (m^2/g)	S/Ti atomic ratio		Surface/bulk S ratio
	XPS	EDS			Surface	Bulk	
E33W67	23/100	4.53/100	1.72	6.67	23/100	3.84/100	5.99/1
E80W20	25/100	6.50/100	2.45	2.86	25/100	6.21/100	4.03/1

* S content determined by EDS.
** SA - surface area determined by N_2 sorption.

Table 7

The average radius of the secondary particles of E33W67 were calculated using equation (4).

Average radii of aggregate/agglomerate: $r = \frac{3}{6.67 \frac{m^2}{g} \times 0.78 \times 10^6 \frac{g}{m^3}} = 576.6\ nm$ (4)

Where 6.67 m^2/g is the measured BET surface area of E33W67 and 0.78×10^6 g/m^3 is the measured bulk density of E33W67. Equation (4) is derived from the BET surface area and assuming that the secondary particles form a perfect sphere.

Assuming that the penetration depth of XPS is approximately 7 nm, the volumes of the outer and inner shells of the secondary particle can be calculated, based upon the radius calculated above, resulting in a surface volume of 3.60% of the total volume.

Equation (5) can then be used to calculate the bulk S/Ti ratio, as the surface S/Ti ratio has been provided by XPS (23/100).

(Surface shell S/Ti ratio x surface shell volume %) + (Inner core S/Ti ratio x inner core volume %) = whole sphere S/Ti ratio x 100% **(5)**

Solving equation 5 for E33W67, provides an inner core S/Ti ratio of 3.84, resulting in a surface/bulk ratio of 5.99/1.

Similar calculations based upon the same assumptions were used to calculate that the radius of the secondary particles of E80W20 was 1345 nm, that its inner core S/Ti ratio was 6.21 and, therefore, its surface/bulk ratio was 4.03/1.

Band Gap Measurements

Semiconductor optical band baps could be measured by UV-Vis diffuse reflectance spectroscopy (DRS). In some cases, band gaps can be directly taken from the raw UV-Vis DRS spectra. Fig. 9a shows UV-Vis DRS spectra of SO_4^{2-}/TiO_2 photocatalysts E0W100, E20W80, E33W67, E50W50, E67W33, E80W20, E100W0 and Degussa P25 TiO_2. At 220 and 288 nm there are charge transfers from O^{2-} to Ti^{4+}. 340 nm is an interband transition for anatase. Fig. 9a indicates that these photocatalysts start to absorb lights at 350 ~ 450 nm. In most cases, it is difficult to decide band gaps directly from the raw UV-Vis DRS spectra due to some reasons such as curve change gradually. Therefore, Tauc plots derived from UV-Vis DRS spectra are used to measure band gaps. Tauc plot function is as in equation (6). In UV-Vis DRS not-transparent powder absorbance coefficient α are usually converted to reflectance using Kubelka-Munk function as equation (7). Resulted final Tauc plot function is equation (8).

$$(h\lambda\alpha)^{\frac{1}{n}} = A\left(h - E_g\right) \quad (6)$$

$$F\left(R_\infty\right) = \frac{(1-R_\infty)}{2R_\infty} = \frac{K}{S} \quad (7)$$

$$(h\upsilon F(R_\infty))^{\frac{1}{n}} = A(h\upsilon - E_g) \quad (8)$$

h – Plank's constant 6.63×10^{-34} J·S; υ – light frequency; α, K – absorbance coefficient; n – denotes the nature of sample transition, for direct allowed transition n = 1/2, for direct forbidden transition n = 3/2, for indirect allowed transition n = 2, for indirect forbidden transition n = 3; A – proportional constant; E_g – band gap; R_∞ - reflectance of infinite layer; S – scattering coefficient. Fig. 9b shows Tauc plot $(hvF(R_\infty))2 \sim h\upsilon$ for direct band gap when n = 1/2 for of SO_4^{2-}/TiO_2 photocatalysts E0W100, E20W80, E33W67, E50W50, E67W33, E80W20, E100W0 and Degussa P25 TiO_2. Direct band gap is for direct vertical transitions from maximum of valence band (O^{2-}) to minimum of conduction band (Ti^{4+}) through optical excitation by absorbing photons.

Fig. 9c shows Tauc plot $(hvF(R_\infty))1/2 \sim h\upsilon$ for indirect band gap when n = 2. Indirect band gap is for phonon assisted transitions involving both photons and phonons together. Usually to decide whether direct band gap or indirect band gap is to be used the linearity of Tauc plot should be considered. The Tauc plot with more linearity should be used. Compare Fig. 9b

and 9c, it is easy to find that Fig. 9c Tauc plot for indirect band gap is more linear than Fig. 9b for direct band gap. Therefore, Fig. 9c should be used to calculate the E_g. Both direct and indirect band gap energies and their equivalent UV light wavelengths for SO_4^{2-}/TiO_2 photocatalysts E0W100, E20W80, E33W67, E50W50, E67W33, E80W20, E100W0 and Degussa P25 TiO_2 are summarized in Table 8. Table 8 shows direct band gap energy is 0.15 ~ 0.2 eV higher than indirect band gap for SO_4^{2-}/TiO_2 photocatalysts. But for Degussa P-25, direct band gap is 0.42 eV higher than that of indirect band gap. Indirect band gaps for SO_4^{2-}/TiO_2 photocatalysts and Degussa P25 are 3.2 ± 0.075 eV, with small differences among them. The equivalent UV light wavelengths of direct and indirect band gap energies are also listed in (Table 8), to compare them with the UV light wavelength (365 nm) used for photocatalytic degradation. From the comparison, it is clear that UV lights with wavelength < 397.8 nm are suitable for the photocatalytic degradation of RO concentrate over SO_4^{2-}/TiO_2 photocatalysts E0W100, E20W80, E33W67, E50W50, E67W33, E80W20, E100W0 and Degussa P25.

Band Gaps	**E100W0**	**E80W20**	**E67W20**	**E50W50**	**E33W67**	**E20W80**	**E0W100**	**Degussa P25**
Direct Band Gap (eV)	3.390	3.320	3.310	3.345	3.380	3.425	3.400	3.625
Wavelength (nm) [a]	366.7	374.4	375.6	371.6	367.8	363.0	365.6	342.9
Indirect Band Gap (eV)	3.195	3.125	3.125	3.170	3.205	3.260	3.245	3.205
Wavelength (nm) [b]	389.1	397.8	397.8	392.2	387.9	381.3	383.1	387.9

a Equivalent UV light wavelength for direct band gap

b Equivalent UV light wavelength for indirect band gap

Table 8

Figure 10 compares the band gap of E20W80 (catalyst #3) to the band gap catalyst 101212B, which is identical to E20W80, except that it was subjected to calcination for 4 hours at 400 °C, instead of for 1 hour. As shown in the figure, the band gaps are not significantly affected by calcination time.

Photocatalyst Morphology

TEM of SO_4^{2-}/TiO_2 photocatalysts prove that they are composed of primary sphere shape nano-size particles (Fig. 11c). Under SEM, secondary particles could be viewed (Fig 11a, 11b). Secondary particles are agglomerates (physically-bound particles; rigidly) or aggregates (chemically or sinter-bound particles; loosely) of primary nanoparticles. Their secondary particles are mainly in the range of 0.02 ~ 3 μm. From Fig. 11a and Fig. 11b, E20W80 secondary particles size distribution has more weight on smaller sizes while E67W33 doesn't. This could be reason that E20W80 has higher BET surface area than E67W33 since they have similar average size of primary nanoparticles (6.3 nm for E20W80; 5.0 nm for E67W33). Degussa P25 TiO_2 shows primary particle size 20 ~ 50 nm under SEM and seldom have secondary particles. High resolution TEM (HRTEM) [54, 55] image of E20W80 (Fig. 11d) shows atomic array of crystal plane (200) along the direction [002]. Using "profile of view" mode, the d(200) spacing was directed measured to be 0.189 nm. Ten d(200) spacing was measured together (so that less measuring error) to be 1.890 nm so each d(200) spacing is 0.189 nm, which is consistent with the d(200) spacing data from powder XRD (Table 2). Selected area electron diffraction (SAED) of E20W80 was performed with 300 keV, the diffraction pattern shows 6 rings (Fig. 11e). d-spacing can be calculated from SAED ring radius according to equation (9). In this figure, the scale unit is 1/nm, which already takes into account of camera length and electron wavelength used in the experiment and pixel conversion of them. Electron wavelength λ can also be calculated using equation (10).

$$d = \lambda . \frac{L}{r} \qquad (9)$$

$$f = \sqrt{\frac{1.5}{(V+10^{-6}V^2)}} \qquad (10)$$

d - the spacing of planes; L - camera length; r – ring radius; λ - electron wavelength; V – electron accelerating voltage.

The ring radius (r) was measured by "profile of frame", the reciprocal of radius r (1/r) was taken as the corresponding d spacing. Starting from inner rings, 1st 2nd 4th 5th 6th ring radius r is 2.854, 4.227, 5.291, 5.964, and 6.774/nm; d spacing (1/r) is calculated to be 3.504, 2.367, 1.890, 1.677, and 1.476 Å. 1st 2nd 4th 5th 6th ring represents plane (101), (004),

(200), (105) + (211), and (118), respectively. 3rd ring is neither anatase nor rutile, unknown. SAED data agrees well with powder XRD data and confirms the anatase crystal phase in SO_4^{2-}/TiO_2 photocatalysts.

Example 4

Catalysts were prepared using General Procedure 1, wherein the hydrolysis was conducted using a ratio of 20:80 ethanol:water (E:W) at 90 °C for 6 hours, and the calcination conditions were varied as listed in Table 9 below. Table 9 also lists the particle sizes of the various materials, the S content by weight and the BET Surface Area (m^2/g) obtained for the resulting particles, as obtained by use of the methods discussed hereinbefore.

Sample ID	Preparation Conditions	Particle Size (nm)	S Content by wt%	BET Surface Area (m^2/g)
#080513A	Calc. 100 °C 1 hr	5.45	1.43	73.9
#090513B	Calc. 200 °C 1 hr	5.64	1.28	144.6
#080513B	Calc. 300 °C 1 hr	5.76	1.19	154.9
#201212A (E20W80)	Calc. 400 °C 1 hr	5.97	1.06	146.9
#080513C	Calc. 500 °C 1 hr	7.33	0.81	134.3
#080513D	Calc. 600 °C 1 hr	12.03	0.24	69.7
#180214A	Calc. 700 °C 1 hr	24.42	<0.1%	31.2
#180214B	Calc. 800 °C 1 hr	44.76	<0.1%	2.7

Table 9

Example 5

The catalysts prepared in Example 4 were then used in the photocatalytic degradation of ROC according to General Procedure 2 for a time of 6 hours. The accumulated conversion rate of the DOC after 6 hours, compared to the particles size is shown in Figure 12 and in Table 10.

As indicated in Table 10 and Figure 12, it appears that the best primary particle size of the titanium nanocatalysts is approximately 12 nm, though a range of from 9 to 26 nm appears to provide improved performance compared to other primary particle size ranges.

Sample ID	Particle Size (nm)	Conversion (%)
#080513A	5.45	62.28
#090513B	5.64	71.94
#080513B	5.76	66.77
#201212A (E20W80)	5.97	81.14
#080513C	7.33	83.25
#080513D	12.03	93.02
#180214A	24.42	89.27
#180214B	44.76	29.17

Table 10

Comparison of the rate of conversion achieved by catalyst #080513D to Degussa P25 over the course of 6 hours (illustrated in Table 11), shows that the catalyst is up to 5 times more active than Degussa P25 over a period of 2 hours and results in a reduction in DOC of 93% compared to 41.2% for Degussa P25 at 6 hours.

Reaction time (hr)	DOC Conv. (%)		Rate Ratio (#080513D :P25)
	Degussa P25	#080513D	
0	0.0	0	NA
0.1	9.7	14.1	1.5 :1
1	11.0	45.5	4.1 :1
2	13.8	68.8	5.0 : 1
4	26.1	86.4	3.3 : 1
6	41.2	93.0	2.3 : 1

Table 11

Claims

1. A composition comprising:
TiO_2 nanocrystals in the form of agglomerates and/or aggregates; and
an anionic species associated with the TiO_2 agglomerates/aggregates, wherein
the diameter of the TiO_2 agglomerates/aggregates is from 0.02 μm to 5.0 μm;
the diameter of the TiO_2 nanocrystals is from 4 to 70 nm; and
the BET surface area of the composition is from 6 to 250 g/m^2.

2. The composition according to Claim 1, wherein the TiO_2 nanocrystals are substantially in the anatase form.

3. The composition according to Claim 1, wherein the anionic species is selected from one or more of the group consisting of SO_4^{2-}, Cl^-, F^-, Br^-, I^-, PO_4^{3-}, NO_3^-, BO_3^{3-}, and SiO_3^{2-}.

4. The composition of Claim 3, wherein, when the anionic species is SO_4^{2-}:
Ti is present in an amount of from 50.9 wt% to 63.9 wt%; and/or
O is present in an amount of from 36.09 wt% to 44.5 wt%; and/or
S is present in an amount of from 0.01 wt% to 4.6 wt%.

5. The composition of Claim 3, wherein, when the anionic species is SO_4^{2-}, the composition has FTIR peaks at approximately 3620-3850 cm^{-1}, 3159 cm^{-1}, 1400 cm^{-1}, 1215 cm^{-1}, 1148 cm^{-1}, 1051 cm^{-1} and 980 cm^{-1}.

6. The composition according to Claim 1, wherein:
the diameter of the agglomerates/aggregates is from 0.05 μm to 3.0 μm; and/or
the diameter of the TiO_2 nanocrystals is from 5 to 50 nm.

7. The composition according to Claim 1, wherein the BET surface area of the composition is from 6.0 to 9.0 g/m^2, or from 20.0 to 90.0 g/m^2 or from 115 to 250 g/m^2.

8. The composition according to Claim 1, wherein the majority of the anionic species is associated with the surface of the TiO_2 agglomerates/aggregates.

9. The composition according to Claim 8, wherein the ratio of the anionic species on the surface of the TiO_2 agglomerates/aggregates compared to the anionic species within the interior volume of the TiO_2 agglomerates/aggregates is from 1.5:1 to 30:1.

10. The composition according to Claim 1, wherein 0.1 wt% of the composition reduces the dissolved organic carbon in 99.9 wt% of reverse osmosis concentrate by from 70% to 80% after 6 hours of photocatalytic reaction.

11. A method of preparing TiO_2 nanocrystals, the method comprising the steps of:

(a) hydrolysing a titanium source in a water/solvent mixture to form a hydrous TiO_2 material;

(b) filtering the hydrous TiO_2 material and washing the filtered hydrous TiO_2 material with a washing solution;

(b) drying and grinding the filtered and washed hydrous TiO_2 material into a powder;

(c) calcinating the powder to form anhydrous TiO_2 nanocrystals; and

(d) optionally further grinding the anhydrous TiO_2 nanocrystals.

12. The method of Claim 11, wherein the titanium source is one or more of the group selected from titanyl sulfate, $TiCl_3$, $TiCl_4$, oxalotitanic acid, titanium ethoxide, titanium n-propoxide, titanium isopropoxide, and titanium n-butoxide.

13. The method of Claim 11, wherein the hydrolysis is conducted at from 25 to 190°C and/or the calcination step is conducted at a temperature of from 100°C to 1000°C using a temperature ramp of from 0.1°C to 100°C per minute for from 0.1 to 48 hours..

14. The method of any one of Claim 11, wherein the solvent used in the hydrolysis reaction is one or more selected from methanol, ethanol, n-propanol, isopropanol, acetone, acetylacetone, methyl ethyl ketone, methyl propyl ketone, methyl isobutyl ketone, methyl pentyl ketone, butyrolactone, methyl formate, ethyl formate, propyl formate, butyl formate, methyl acetate, oxaloacetate, ethyl acetate, propyl acetate, butyl acetate, and dibasic ester.

15. The method of Claim 11, wherein the water/solvent ratio is from 1:10 to 20:1 or only water is used and/or the weight ratio of the titanium source to the solvent/water in the hydrolysis step is from 1:1000 to 10:1.

16. The method of Claim 11, wherein the washing solution is selected from one or more of 0.01 to 5 M ammonia (aq), methanol, ethanol, isopropanol, acetone, methyl ethyl ketone, methyl isobutyl ketone, methyl formate, ethyl formate, methyl acetate, and ethyl acetate.

17. The method of Claim 11, wherein step (a) further comprises adding a anionic source to the titanium source and water/solvent mixture, optionally wherein the anionic source contains one or more (or is capable of producing one or more) anions selected from the group consisting of F^-, Br^-, I^-, PO_4^{3-}, NO_3^-, BO_3^{3-}, and SiO_3^{2-}.

18. A composition made by the process of Claim 11.

19. Use of the composition Claim 1 or Claim 18 as a photocatalyst.

20. The use of Claim 19, wherein the photocatalyst is used for:
the treatment of any one of wastewater, drinking water and ROC;
air purification; or
surface self-cleaning.

FIGURES

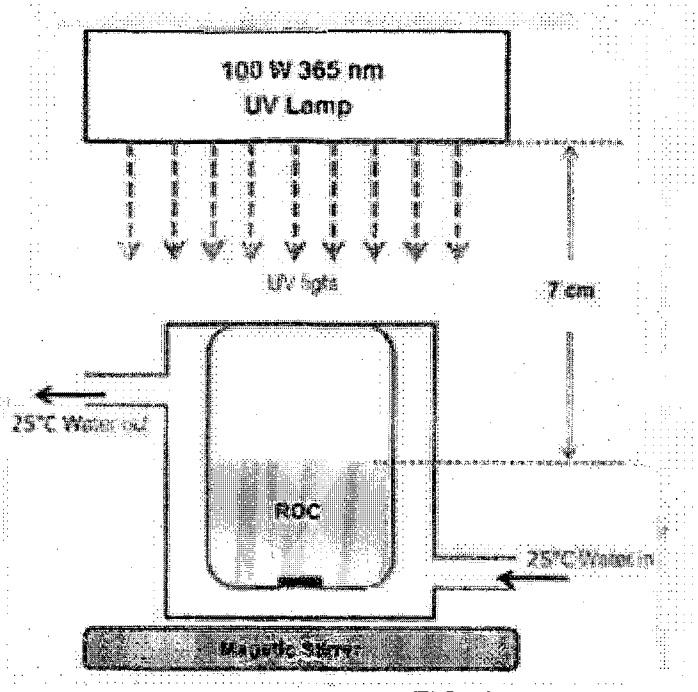


FIG. 1

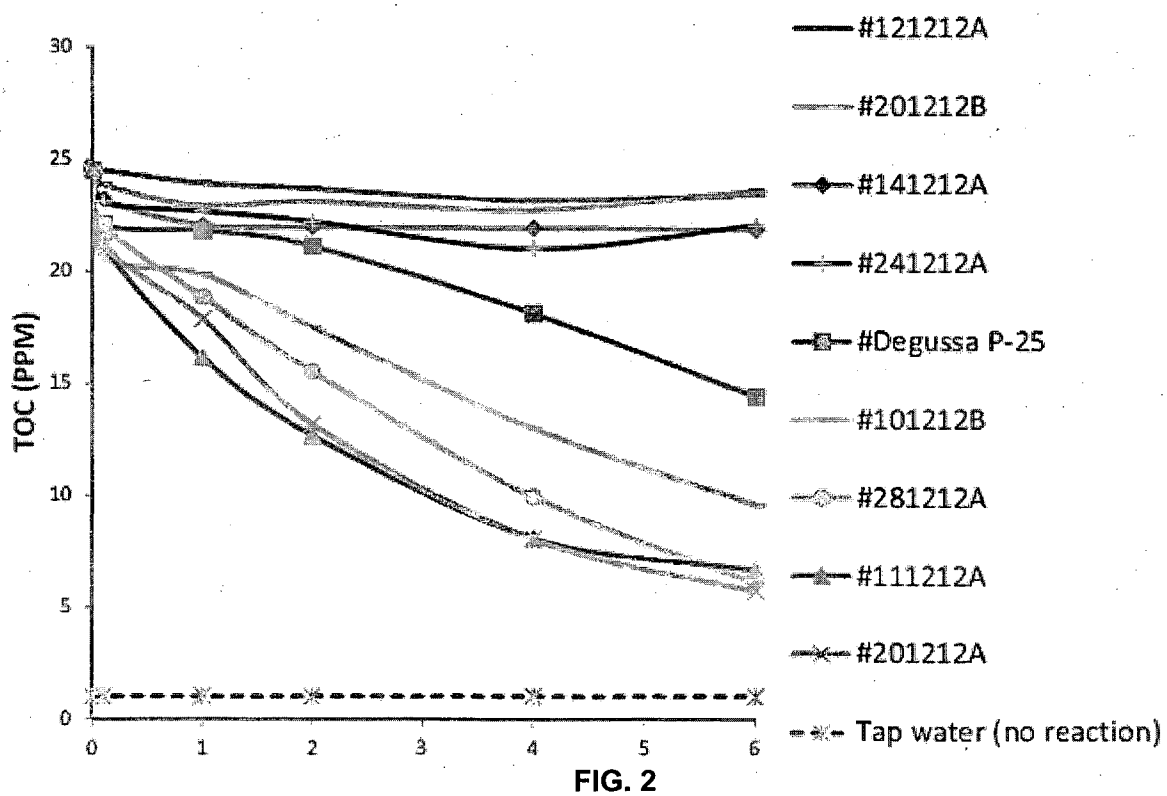


FIG. 2

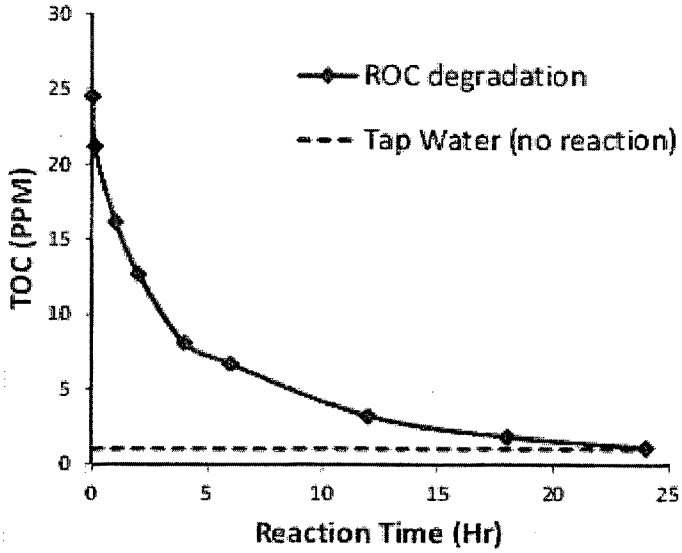

ROC degradation
Tap Water (no reaction)
TOC (PPM)
Reaction Time (Hr)

FIG. 3

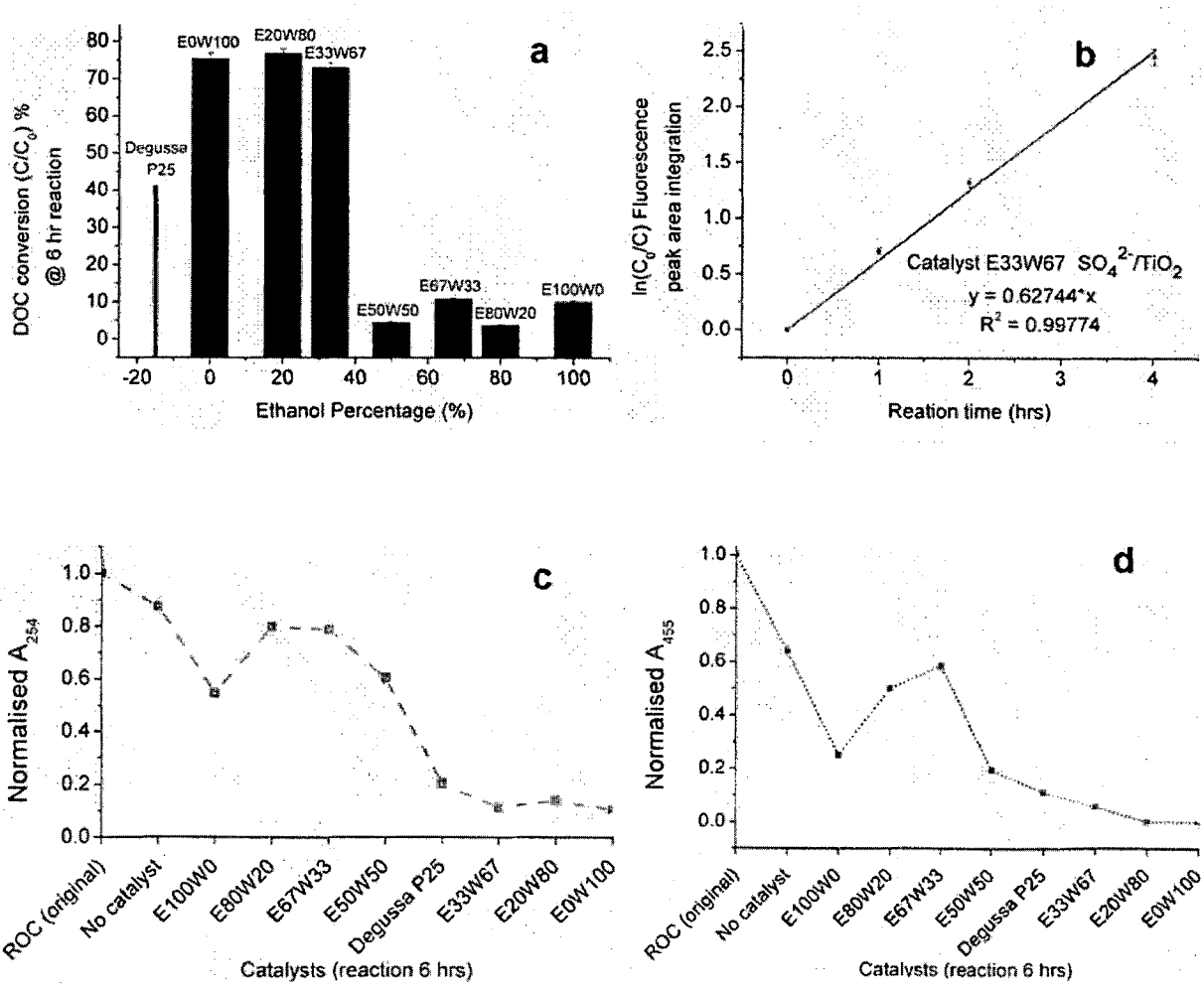

a
DOC conversion (C/C0) % @ 6 hr reaction
Degussa P25
E0W100
E20W80
E33W67
E50W50
E67W33
E80W20
E100W0
Ethanol Percentage (%)
b
ln(C0/C) Fluorescence peak area integration
Catalyst E33W67 SO4 2-/TiO2
y = 0.62744*x
R2 = 0.99774
Reation time (hrs)
c
Normalised A254
ROC (original)
No catalyst
E100W0
E80W20
E67W33
E50W50
Degussa P25
E33W67
E20W80
E0W100
Catalysts (reaction 6 hrs)
d
Normalised A455
Catalysts (reaction 6 hrs)

FIG. 4

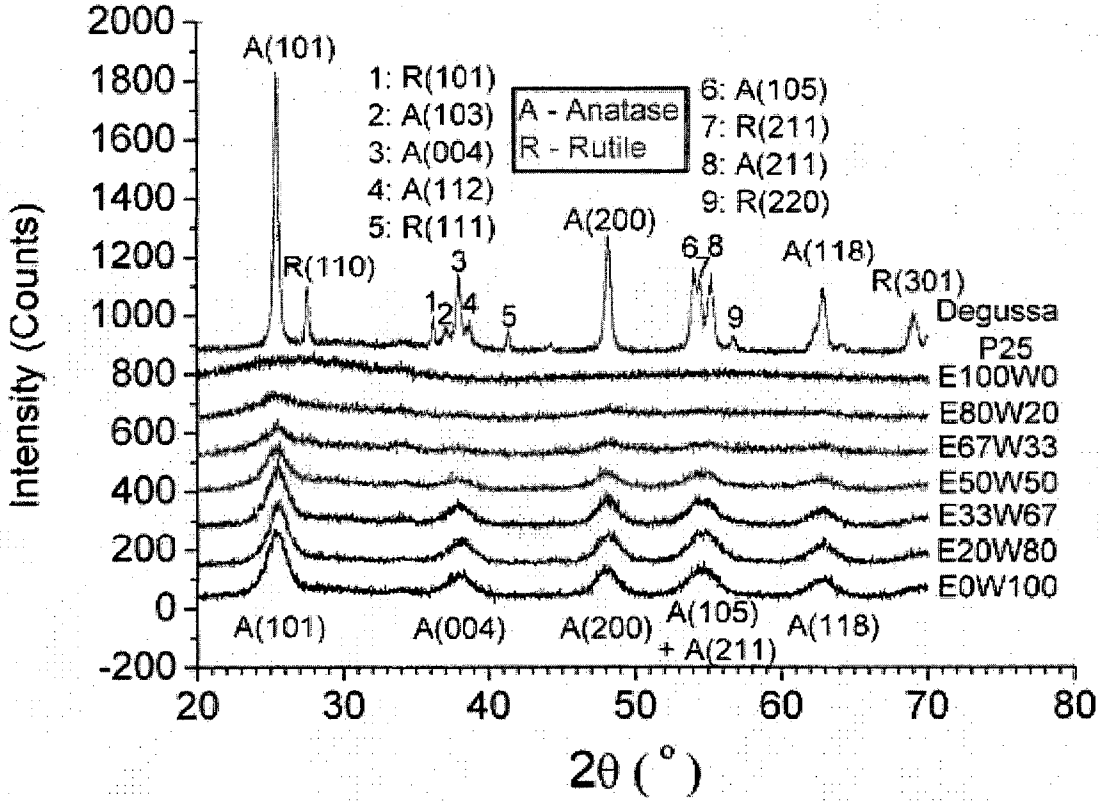

Intensity (Counts)
2θ (°)
A(101)
R(110)
A(200)
A(118)
R(301)
1: R(101)
2: A(103)
3: A(004)
4: A(112)
5: R(111)
6: A(105)
7: R(211)
8: A(211)
9: R(220)
A - Anatase
R - Rutile
Degussa P25
E100W0
E80W20
E67W33
E50W50
E33W67
E20W80
E0W100
A(101)
A(004)
A(200)
A(105) + A(211)
A(118)

FIG. 5

00

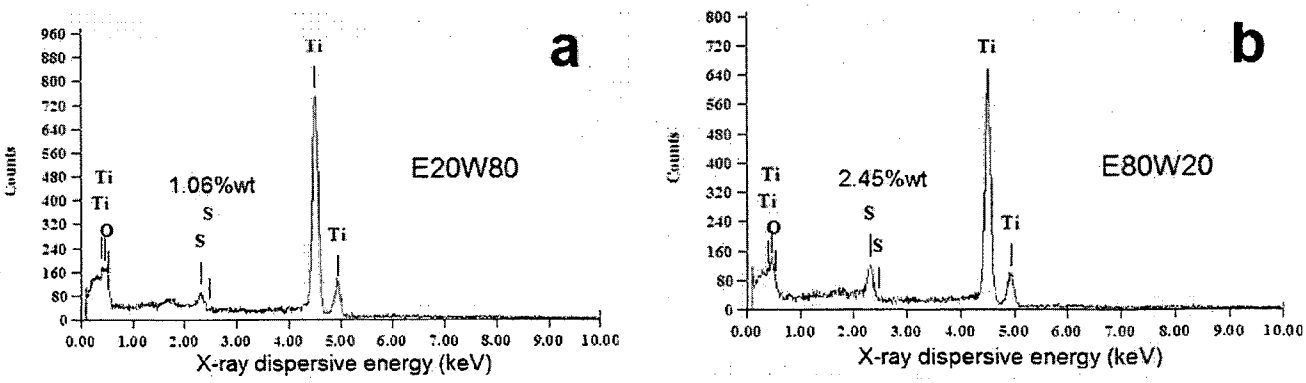

a
E20W80
1.06%wt
Ti
O
S
Counts
X-ray dispersive energy (keV)
b
E80W20
2.45%wt
Ti
O
S
Counts
X-ray dispersive energy (keV)

FIG. 6

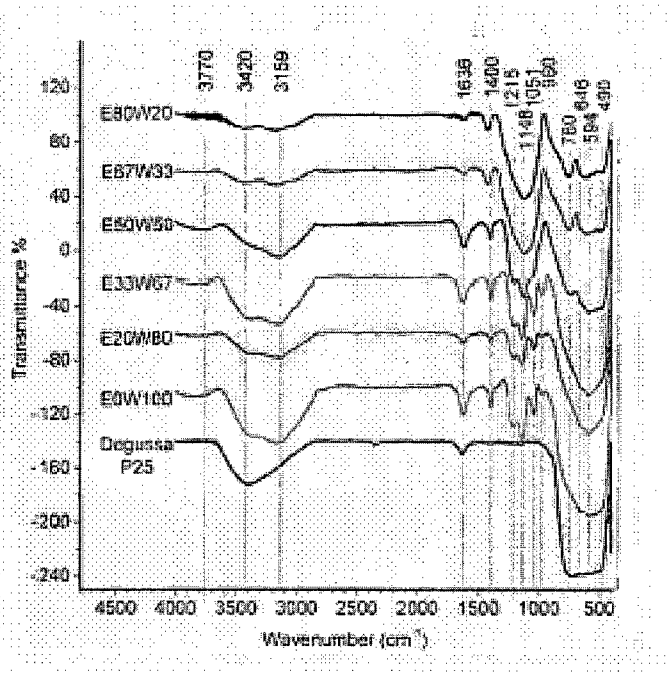

3770
3420
3159
1638
1400
1215
1148
1051
999
780
646
594
490
E80W20
E67W33
E50W50
E33W67
E20W80
E0W100
Degussa P25
Transmittance %
120
80
40
0
-40
-80
-120
-160
-200
-240
4500 4000 3500 3000 2500 2000 1500 1000 500
Wavenumber (cm-1)

FIG. 7

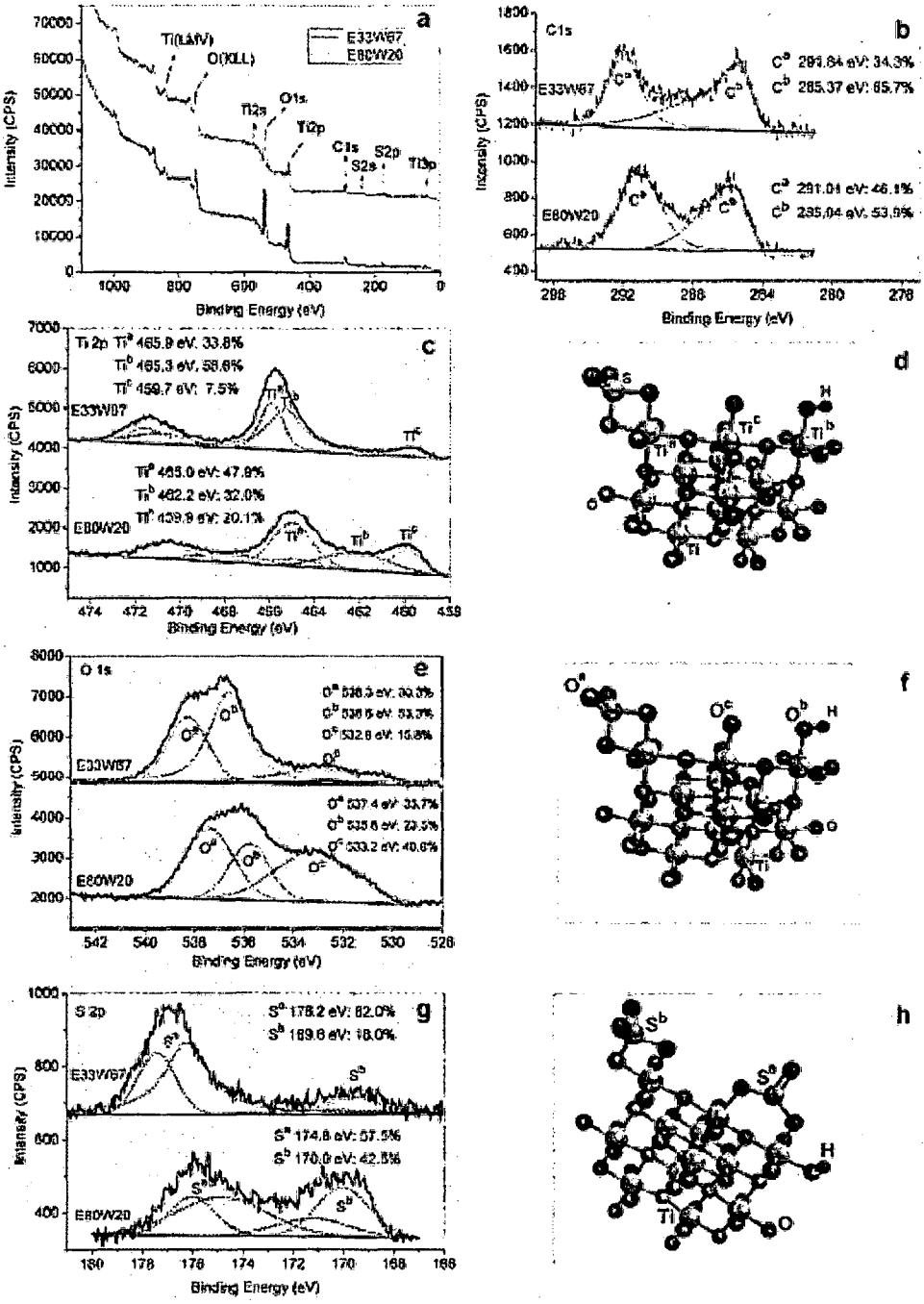

a
Ti(LMV)
O(KLL)
E33W67
E80W20
Ti2s
O1s
Ti2p
C1s
S2p
S2s
Ti3p
Intensity (CPS)
Binding Energy (eV)
b
C1s
E33W67
E80W20
Intensity (CPS)
Binding Energy (eV)
c
Ti 2p
E33W67
E80W20
Intensity (CPS)
Binding Energy (eV)
d
e
O 1s
E33W67
E80W20
Intensity (CPS)
Binding Energy (eV)
f
g
S 2p
E33W67
E80W20
Intensity (CPS)
Binding Energy (eV)
h

FIG. 8

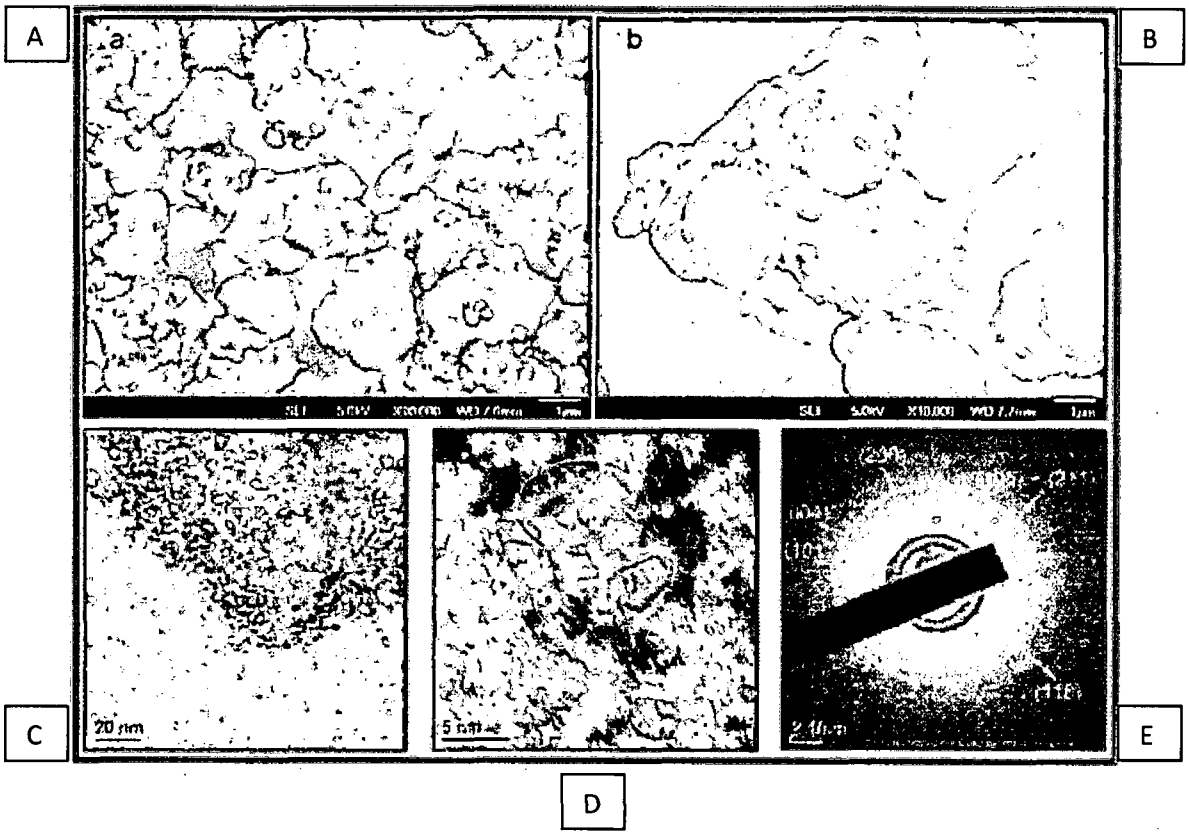

A
B
C
D
E
a
b
20 nm
5 nm

FIG. 9

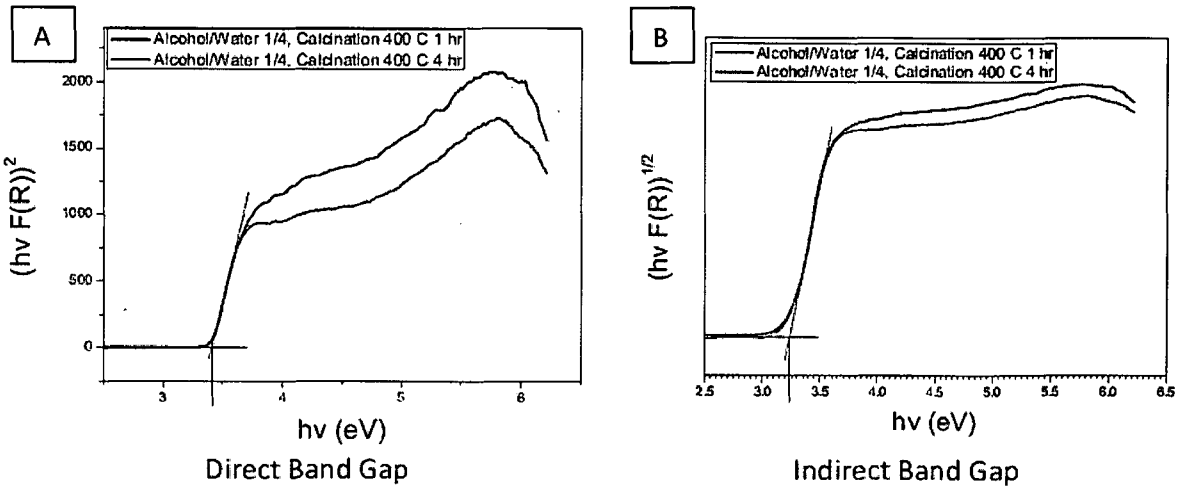

A
Alcohol/Water 1/4, Calcination 400 C 1 hr
Alcohol/Water 1/4, Calcination 400 C 4 hr
(hv F(R))2
hv (eV)
Direct Band Gap
B
Alcohol/Water 1/4, Calcination 400 C 1 hr
Alcohol/Water 1/4, Calcination 400 C 4 hr
(hv F(R))1/2
hv (eV)
Indirect Band Gap

FIG. 10

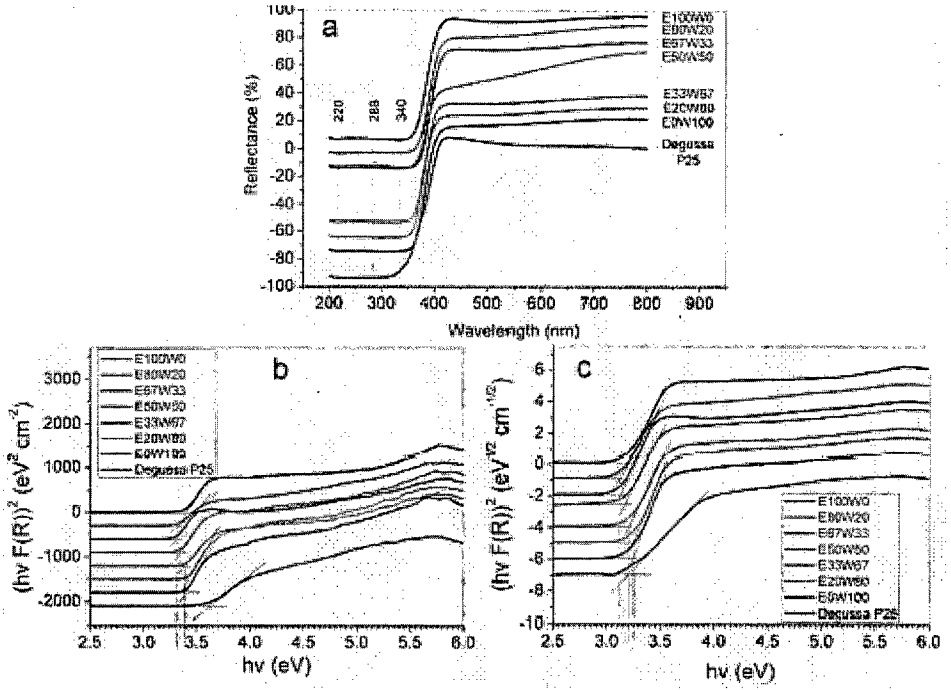

a
Reflectance (%)
Wavelength (nm)
220
288
340
E100W0
E80W20
E67W33
E50W50
E33W67
E20W80
E0W100
Degussa P25
b
(hv F(R))² (eV² cm⁻²)
hv (eV)
c
(hv F(R))² (eV^1/2 cm^-1/2)
hv (eV)

FIG. 11

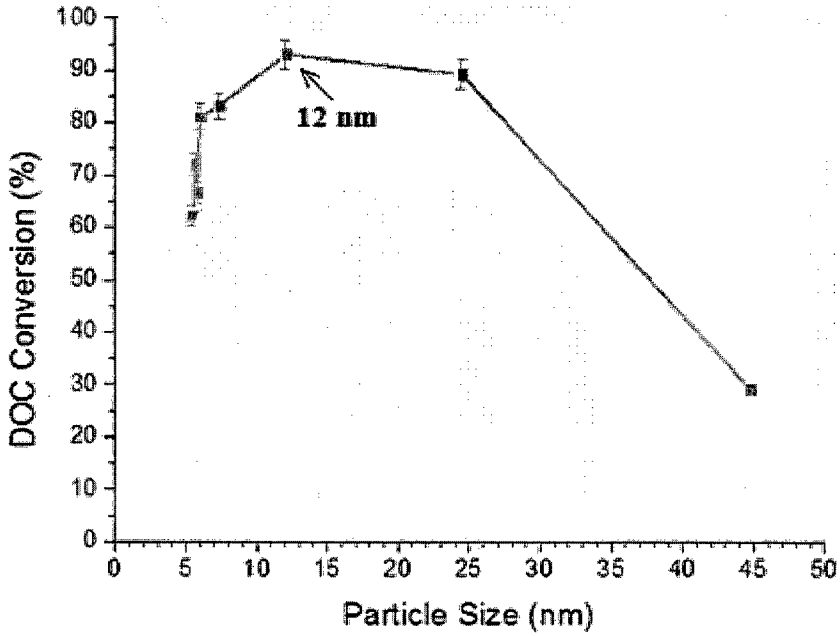

DOC Conversion (%)
Particle Size (nm)
12 nm

FIG. 12

INTERNATIONAL SEARCH REPORT

International application No.
PCT/SG2014/000358

A. CLASSIFICATION OF SUBJECT MATTER

B82Y 30/00 (2011.01) B82B 3/00 (2006.01) B01J 21/06 (2006.01) C02F 1/44 (2006.01) C01G 21/00 (2006.01)

According to International Patent Classification (IPC) or to both national classification and IPC

B. FIELDS SEARCHED

Minimum documentation searched (classification system followed by classification symbols)

Documentation searched other than minimum documentation to the extent that such documents are included in the fields searched

Electronic data base consulted during the international search (name of data base and, where practicable, search terms used)

Databases: GOOGLE PATENTS, GOOGLE SCHOLAR, ESPACENET. AUSPAT, ESPACENET, GOOGLE PATENTS. EPODOC, WPI, INSPEC

Keywords: TiO2, So4, nanoparticles, nanocrystals, surface area, FTIR, anatase, anionic, reverse osmosis, water filtration, photocatalyst and similar terms. **Applicant/Inventor Search:** NUS, National University Singapore // Sam Fong Yau LI, Xuan Hao LIN

C. DOCUMENTS CONSIDERED TO BE RELEVANT

Category*	Citation of document, with indication, where appropriate, of the relevant passages	Relevant to claim No.
	Documents are listed in the continuation of Box C	

[X] Further documents are listed in the continuation of Box C [X] See patent family annex

* Special categories of cited documents:

"A" document defining the general state of the art which is not considered to be of particular relevance

"E" earlier application or patent but published on or after the international filing date

"L" document which may throw doubts on priority claim(s) or which is cited to establish the publication date of another citation or other special reason (as specified)

"O" document referring to an oral disclosure, use, exhibition or other means

"P" document published prior to the international filing date but later than the priority date claimed

"T" later document published after the international filing date or priority date and not in conflict with the application but cited to understand the principle or theory underlying the invention

"X" document of particular relevance; the claimed invention cannot be considered novel or cannot be considered to involve an inventive step when the document is taken alone

"Y" document of particular relevance; the claimed invention cannot be considered to involve an inventive step when the document is combined with one or more other such documents, such combination being obvious to a person skilled in the art

"&" document member of the same patent family

Date of the actual completion of the international search	Date of mailing of the international search report
28 October 2014	28 October 2014
Name and mailing address of the ISA/AU	**Authorised officer**
AUSTRALIAN PATENT OFFICE PO BOX 200, WODEN ACT 2606, AUSTRALIA Email address: pct@ipaustralia.gov.au	ISAAC TAN AUSTRALIAN PATENT OFFICE (ISO 9001 Quality Certified Service) Telephone No. 0262832814

INTERNATIONAL SEARCH REPORT C (Continuation). DOCUMENTS CONSIDERED TO BE RELEVANT		International application No. **PCT/SG2014/000358**
Category*	Citation of document, with indication, where appropriate, of the relevant passages	Relevant to claim No.
X	CN 102416333 A (中国科学院广州能源研究所) 18 April 2012 Abstract, [0020 - 0055])	1 - 10, 19 - 20 (in part)
X	Su, W. Y. et al., "Effect of Sulfation on Structure and Photocatalytic Performance of TiO_2", Acta Phys. Chim. Sin., Vol 17 No 1, 2001, Pages 28 - 31 Abstract, Table 1	1 - 3, 5 - 7, 10 & 19 - 20 (in part)
A	Wang, X. C. et al., "Probing of photocatalytic surface sites on SO_4^{2-}/TiO_2 solid acids by in situ FT-IR spectroscopy and pyridine adsorption", Journal of Photochemistry and Photobiology A: Chemistry, Vol 179, 2006, Pages 339 - 347 Figure 5	5
A	CN 1636879 A (攀钢集团攀枝花钢铁研究院 et al.) 13 July 2005 Whole Document	1 - 10, 19 - 20 (in part)
A	Jiang, X. Y. et al., "Preparation of nano-TiO_2 photocatalysts and their decomposition activity in phenol-contaminated water", Journal of Zhejiang University Science A, Vol 10 Issue 11, 2009, Pages 1651 - 1659 Whole Document	1 - 10, 19 - 20 (in part)
A	CN 1762581 A (鞍山科技大学) 26 April 2006 Whole Document	1 - 10, 19 - 20 (in part)
A	WO 2009/113045 A2 (Dublin Institute of Technology) 17 September 2009 Whole Document	1 - 10, 19 - 20 (in part)

INTERNATIONAL SEARCH REPORT

International application No.
PCT/SG2014/000358

Box No. II Observations where certain claims were found unsearchable (Continuation of item 2 of first sheet)

This international search report has not been established in respect of certain claims under Article 17(2)(a) for the following reasons:

1. ☐ Claims Nos.:

because they relate to subject matter not required to be searched by this Authority, namely:

the subject matter listed in Rule 39 on which, under Article 17(2)(a)(i), an international search is not required to be carried out, including

2. ☐ Claims Nos.:

because they relate to parts of the international application that do not comply with the prescribed requirements to such an extent that no meaningful international search can be carried out, specifically:

3. ☐ Claims Nos:

because they are dependent claims and are not drafted in accordance with the second and third sentences of Rule 6.4(a)

Box No. III Observations where unity of invention is lacking (Continuation of item 3 of first sheet)

This International Searching Authority found multiple inventions in this international application, as follows:

See Supplemental Box for Details

1. ☐ As all required additional search fees were timely paid by the applicant, this international search report covers all searchable claims.

2. ☐ As all searchable claims could be searched without effort justifying additional fees, this Authority did not invite payment of additional fees.

3. ☐ As only some of the required additional search fees were timely paid by the applicant, this international search report covers only those claims for which fees were paid, specifically claims Nos.:

4. ☒ No required additional search fees were timely paid by the applicant. Consequently, this international search report is restricted to the invention first mentioned in the claims; it is covered by claims Nos.:

1 - 10 & 19 - 20 (in part)

Remark on Protest

☐ The additional search fees were accompanied by the applicant's protest and, where applicable, the payment of a protest fee.

☐ The additional search fees were accompanied by the applicant's protest but the applicable protest fee was not paid within the time limit specified in the invitation.

☐ No protest accompanied the payment of additional search fees.

Supplemental Box

Continuation of: **Box III**

This International Application does not comply with the requirements of unity of invention because it does not relate to one invention or to a group of inventions so linked as to form a single general inventive concept.

This Authority has found that there are different inventions based on the following features that separate the claims into distinct groups:

- Claims 1 - 10 & 19 - 20 (in part) is directed towards a composition of TiO2 nanocrystals in the form of agglomerates and/or aggregates; and an anionic species associated with the TiO_2 agglomerates/aggregates, with a specific diameter of the agglomerates/aggregates, individual nanocrystals and BET surface area.
- Claims 11 - 18 & 19 - 20 (in part) is directed towards a method of preparing TiO_2 nanocrystals, the method comprising the steps of; hydrolysis, filtration, drying, calcinating and [optionally] further grinding.

PCT Rule 13.2, first sentence, states that unity of invention is only fulfilled when there is a technical relationship among the claimed inventions involving one or more of the same or corresponding special technical features. PCT Rule 13.2, second sentence, defines a special technical feature as a feature which makes a contribution over the prior art.

When there is no special technical feature common to all the claimed inventions there is no unity of invention.
In the above groups of claims, the identified features may have the potential to make a contribution over the prior art but are not common to all the claimed inventions and therefore cannot provide the required technical relationship. The only feature common to all of the claimed inventions is that they both refer to TiO_2 nanocrystals.

However it is considered that this feature is generic in this particular art. In particular, although the method of claim 11 may result in the synthesis of TiO_2 nanocrystals, the claim is unduly broad & there is nothing to suggest that this will obtain TiO_2 nanocrystals having the very specific dimensions as recited in claim 1. For example, precise control over the ratio of precursors, choice of solvent or even the calcinating temperature needs to be carefully determined as very small changes in the variables can have an adversed impact on the dimensions of the synthesised nanocrystals.

Therefore this common feature cannot be a special technical feature. Hence there is no special technical feature common to all the claimed inventions and the requirements for unity of invention are consequently not satisfied a *priori*.

It is considered that search and examination for the second invention will require more than negligible additional search and examination effort over that for the first invention, and therefore an additional search fee is warranted.

INTERNATIONAL SEARCH REPORT Information on patent family members	International application No. **PCT/SG2014/000358**

This Annex lists known patent family members relating to the patent documents cited in the above-mentioned international search report. The Australian Patent Office is in no way liable for these particulars which are merely given for the purpose of information.

Patent Document/s Cited in Search Report		**Patent Family Member/s**	
Publication Number	**Publication Date**	**Publication Number**	**Publication Date**
CN 102416333 A	18 April 2012	CN 102416333 B	22 May 2013
CN 1636879 A	13 July 2005	None	
CN 1762581 A	26 April 2006	None	
WO 2009/113045 A2	17 September 2009	EP 2257374 A2	08 Dec 2010
		IE 20090181 A1	28 Oct 2009
		US 2011028311 A1	03 Feb 2011
		US 8551909 B2	08 Oct 2013

End of Annex

Due to data integration issues this family listing may not include 10 digit Australian applications filed since May 2001.